ACS Chemical Neuroscience

Article

Design, Green Synthesis of Piperlongumine Analogs and Their Antioxidant Activity against Cerebral Ischemia-reperfusion Injury

Ge Li, Yuantie Zheng, Jiali Yao, Linya Hu, Qunpeng Liu, Furong Ke, Weixiao Feng, Ya Zhao, Pengcheng Yan, Wenfei He, Hui Deng, Peihong Qiu, Wulan Li, and Jianzhang Wu

ACS Chem. Neurosci., **Just Accepted Manuscript** • DOI: 10.1021/acschemneuro.9b00402 • Publication Date (Web): 06 Sep 2019

Just Accepted

is published by the American Chemical Society. 1155 Sixteenth Street N.W., Washington, DC 20036

Design, Green Synthesis of Piperlongumine Analogs and Their Antioxidant Activity against Cerebral Ischemia-Reperfusion Injury

Ge Li[a], Yuantie Zheng[a], Jiali Yao[a], Linya Hu[a], Qunpeng Liu[ad], Furong Ke[a], Weixiao Feng[ab], Ya Zhao[ca], Pencheng Yan[a], Wenfei He[a], Hui Deng[c], Peihong Qiu[a], Wulan Li[ba]*, Jianzhang Wu[a]*

([a]Chemical Biology Research Center, School of Pharmaceutical Sciences, Wenzhou Medical Universtiy, Wenzhou, Zhejiang 325035, China)

([b]The First Affiliated Hospital of Wenzhou Medical University, Wenzhou, Zhejiang 325035, China)

([c]Department of Periodontics, Hospital & School of Stomatology, Wenzhou Medical University, No. 373 West Xueyuan Road, Wenzhou, Zhejiang 325035, China)

([d]College of Chemistry and Materials Engineering, Wenzhou University, Wenzhou, Zhejiang 325035, China)

*Correspondence authors.

Address: Chemical Biology Research Center, School of Pharmaceutical Sciences, Wenzhou Medical Universtiy, Wenzhou, Zhejiang 325035, China.

Tel./Tex: +86 577 86689984

E-mail: wjzwzmu@163.com

Address: The First Affiliated Hospital of Wenzhou Medical University, Wenzhou, Zhejiang 325035, China.

Tel./Tex: +86 577 86689916

lwlwzmu@163.com

Disclosures/Conflicts of Interest: None declared

Abstract: The supplementation of exogenous antioxidants to scavenge excessive reactive oxygen species (ROS) is an effective treatment for cerebral ischemia reperfusion injury (CIRI). Piperlongumine (PL) is a kind of natural product which has a great potential as neuroprotective agents, but it also has obvious neurotoxicity. Moreover, its neuroprotective effects remain to be improved. In this study, we designed a series of novel PL analogs by hybridizing the screened low-toxic diketene skeleton with antioxidant effect and the 3,4,5-trimethoxyphenyl group, which may increase the antioxidant activity of PL. The intermediate was synthesized by a novel green synthesis method, and 34 compounds were obtained. All the compounds without obvious cytotoxicity have remarkable antioxidant effects, especially compared with diketene skeletons and PL. The cytoprotection of the

active compound decreased significantly by reduction of the carbon-carbon double bonds of the Michael acceptor in the diketene skeleton. More importantly, further study revealed that compound **A9** which has the best activity can confer protection for cells against oxidative stress and attenuate brain injury in vivo. Overall, this study provided a promising drug candidate for the treatment of CIRI and guide the further development of drug research in oxidative stress-mediated diseases.

Keywords: Piperlongumine; Michael acceptor; Green synthesis; Antioxidation; Oxidative stress; Neuroprotection; Cerebral ischemia-reperfusion injury

1. Introduction

Oxidative stress is increasingly considered as primary causes of neurodegenerative diseases (NDDs) [1-2]. Under pathological conditions, a large number of reactive oxygen species (ROS) were induced by oxidative stress, and the accumulation of excessive ROS can create a state of redox imbalance leading to brain damage [3-4]. Ischemic stroke, one of NDDs, is characterized by the high mortality and disability rate in clinical practice across the world [5]. At present, reperfusion is a major therapy to reverse brain damage after ischemic stroke [6-7], but this treatment could cause secondary cellular and tissue damage that is called cerebral ischemia reperfusion injury (CIRI) [8]. The supplementation of exogenous antioxidants is a promising therapy for the treatment of CIRI. However, there are few approved neuroprotective agents were approved in the clinical therapy [9]. Hence, it is of enormous significance to develop new therapeutic antioxidants with high efficacy and low toxicity.

As a major type of natural products, alkaloids are a group of main sources for drug development. Piperlongumine (PL), a naturally occurring alkaloid from Piper longum L., possesses extensive pharmacological activities such as anti-cancer, anti-inflammatory, anti-angiogenic, anti-plate aggregation, and anti-fungal properties [10-12]. Previous studies have indicated that PL possesses the neuroprotective effect [13-14]. However, its activity and toxicity of PL still need to be further improved. Another study found that the olefinic bond in the α, β-unsaturated amide structure of PL analogs is essential for the cytoprotection in neural cells [15]. Nevertheless, some reports indicate that the α, β-unsaturated ketone structure is a kind of Michael acceptor, which can result in toxicity [16]. To sum up, the above results suggest that both the cytoprotection and cytotoxicity of PL may be concerned with its α, β-unsaturated ketone structure in the molecules of PL. Meanwhile， some compounds (shown in Figure 1B) which contain the α, β-unsaturated ketone structure including two olefinic bonds (namely diketene structure) have excellent protective effects.

[17-20]. While the structure-activity relationship (SAR) between the activity or toxicity of these compounds' skeletons and the types of linking ketones in the diketene skeleton were not clear yet. In our previous work, it was found that the activity and toxicity vary significantly from compounds with the same benzene ring substituents but the different diketene skeletons [21]. It is suggested that the protective activity and toxicity of these compounds may be strongly associated with the different type of linking ketones in the diketene skeletons. Thus, we conducted the SAR research on various diketene skeletons. As shown in Figure 1C, on the one hand, compounds **a** (the linking ketone is cyclopentanone) and **e** (the linking ketone is pyrone) all showed low cytotoxicity compared to others. On the other hand, only **a** (2,5-(dibenzylidene)-cyclopentan-1-one) could display obvious antioxidant effect against H_2O_2 damage in PC12 cells. Moreover, accumulated evidences have confirmed that the compounds (shown in Figure 1A) containing a 3,4,5-trimethoxyphenyl group can be proposed as potential antioxidants [22-24]. Although PL has this structural unit, there are no studies evaluating the relevance of it with the antioxidant activity. In order to reduce the cytotoxicity and improve antioxidant activity of PL, a series of novel PL analogs whose structure are 2-(substituted benzylidene)-5-(3,4,5-trimethoxy benzylidene) cyclopentan-1-one (Figure 1D) were designed by hybridizing skeleton **a** and the 3,4,5-trimethoxyphenyl group. In brief, this research adopted a greener system for synthesizing intermediates using L-proline as the catalyst to obtain a series of PL analogs, and evaluated their antioxidant activities against CIRI.

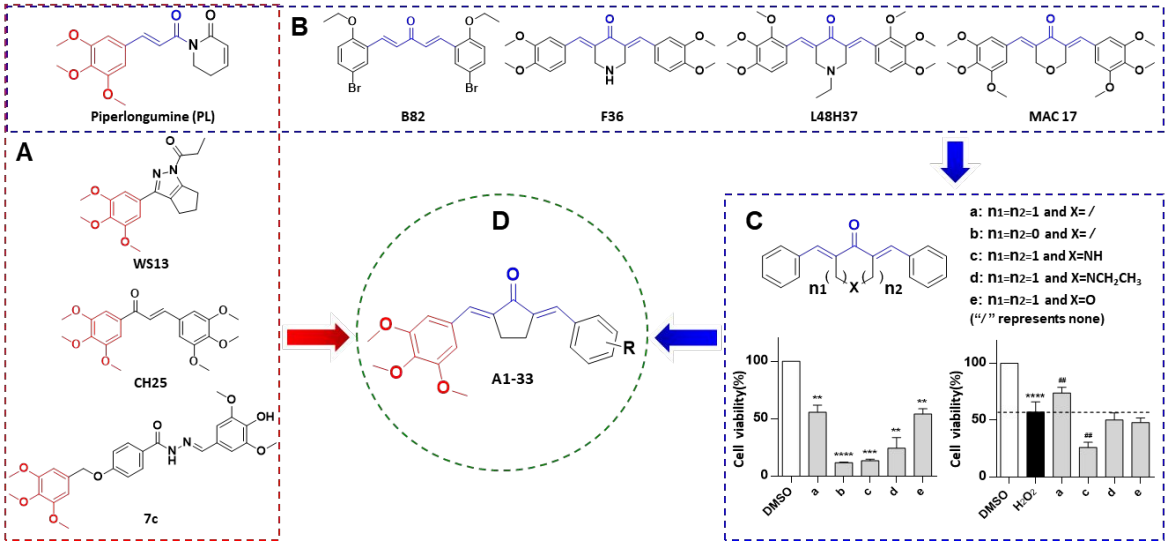

Figure 1. The design of PL analogs (A) The antioxidant compounds bearing a 3,4,5-trimethoxy benzyl moiety (B) The protective agents with the α, β-unsaturated ketone structure which including two olefinic bonds (C) The cytoprotection and cytotoxicity of various diketene skeletons (D) The structure of asymmetric PL analogs

2. RESULTS AND DISCUSSION

2.1 Chemistry

At present, the intermediate's synthesis methods of asymmetric analogues have the disadvantages of cumbersome synthesis steps, environmentally unfriendly and low yield [25-27]. For example, the synthesis of intermediate (E)-2-(benzylidene) cyclopentanone [23], (E)-2-(benzylidene) pyrone [25-26] or (E)-2-(benzylidene) cyclohexanone [27] consist of three steps. ketones are generally protected by morpholine and exposed a single α-H to generate Claisen-Schmidt reaction with aromatic aldehydes. The imine immediate product of this reaction is hydrolyzed under acidic conditions to form the (E)-2-(benzylidene) cycloketone intermediates [23]. Another example is the intermediate (E)-4-phenylbutyl-3-ene-2-ketone, which is synthesized by Claisen-Schmidt reaction. Since strong bases such as NaOH are common catalysts in Claisen-Schmidt reaction [28], the equipment can be corroded and a lot of solid waste were produced. All these above are not in conformity with the concept of Green Chemistry. Hence, it is necessary to find a simple, green and highly efficient synthetic method for asymmetric analogs [29]. We then established a reaction condition taking L-proline as a catalyst for one-step synthesis of intermediate (E)-2-(benzylidene) cyclopentanone (**Scheme 1**). Compared with the previously reported methods, this synthetic method is not only simpler and easier to perform, but also more environment-friendly. To be more specific, A and B series compounds were synthesized by the reaction of the intermediate and substituted benzaldehyde. C and D series compounds were synthesized through hydrogen reduction. All reactions were monitored on the silica gel thin layer chromatography and all compounds were purified by column chromatography. These compounds were obtained in good yields after purification, and their structures were illustrated in **Table 1.** The products were characterized by analysis and comparison of their ^{1}H-NMR and MS spectroscopic data. These characteristic data including color, yield, melting points, MS and ^{1}H-NMR spectra of compounds were presented in chemistry synthetic section. Before being used for the biological experiments, all compounds were purified using re-crystallization or column chromatography.

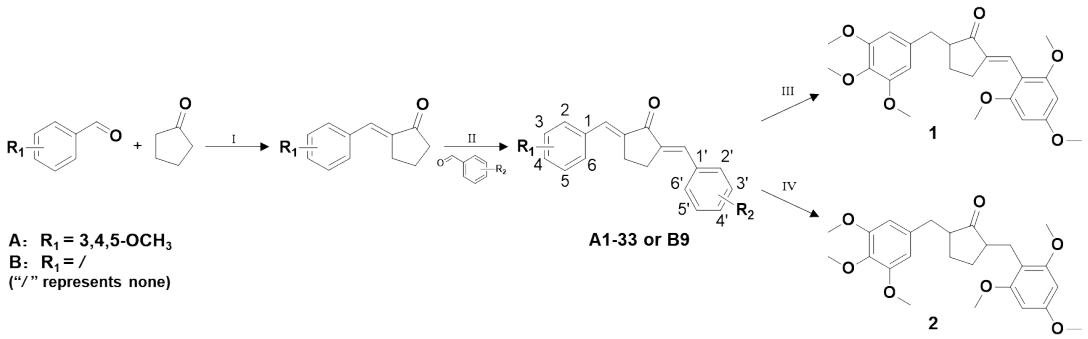

Scheme 1. The general route to produce the asymmetric 1,5-diaryl(substituted)penta-1,4-diene-3-one analogs. Reagents and conditions: (I): a: L-proline, anhydrous dimethylsulfoxide, room temperature; b: Con. HCl, room temperature; (II): 40% NaOH or HCl gas, room temperature; (III): H_2, Pb/C, 12 h , room temperature; (IV): H_2, Pb/C, 24 h , room temperature.

Table 1. The asymmetric 1,5-diaryl(substituted)penta-1,4-diene-3-one analogs

Comp.	R_1	R_2	Comp.	R_1	R_2
A1	3,4,5-OCH_3	2,4-Cl	**A18**	3,4,5-OCH_3	2,5-OCH_3
A2	3,4,5-OCH_3	4-$N(CH_3)_2$	**A19**	3,4,5-OCH_3	2-Br
A3	3,4,5-OCH_3	3-OCH_3, 4-OH	**A20**	3,4,5-OCH_3	4-Cl
A4	3,4,5-OCH_3	4-OCH_3	**A21**	3,4,5-OCH_3	3,4-Cl
A5	3,4,5-OCH_3	2-OH	**A22**	3,4,5-OCH_3	3,4-F
A6	3,4,5-OCH_3	4-OH	**A23**	3,4,5-OCH_3	3,4,5-OCH_3
A7	3,4,5-OCH_3	3-OH	**A24**	3,4,5-OCH_3	3,4-OCH_3
A8	3,4,5-OCH_3	3-F	**A25**	3,4,5-OCH_3	2,3-Cl
A9	3,4,5-OCH_3	2,4,6-OCH_3	**A26**	3,4,5-OCH_3	2-F, 5-OCH_3
A10	3,4,5-OCH_3	3-OH, 4-OCH_3	**A27**	3,4,5-OCH_3	
A11	3,4,5-OCH_3	2,4-OCH_3	**A28**	3,4,5-OCH_3	3,5-OCH_3, 4-OH
A12	3,4,5-OCH_3	2-OCH_3	**A29**	3,4,5-OCH_3	2,6-Cl
A13	3,4,5-OCH_3		**A30**	3,4,5-OCH_3	4-Br
A14	3,4,5-OCH_3		**A31**	3,4,5-OCH_3	3,5-Cl
A15	3,4,5-OCH_3	2,3-OCH_3	**A32**	3,4,5-OCH_3	3-OCH_3
A16	3,4,5-OCH_3	2-CF_3	**A33**	3,4,5-OCH_3	3,5-OCH_3
A17	3,4,5-OCH_3	3,4-OH	**B9**	/	3,4,5-OCH_3

2.2 The cytotoxicity screening and protection of compounds in PC12 cells

In general, ideal antioxidant agents have lower toxicity, so the cytotoxicity of compounds toward the PC12 cells were determined by the MTT assay. As shown in Figure 2A, it is noticeable that most compounds (25 compounds) displayed no prominent toxicity to PC12 cells in comparison with the control group. The other 11 compounds, while showing certain toxicity in PC12 cells, were still much less toxic than PL. In addition, **A1**, **A13**, **A14**, **A27** and **A28** were showed distinct toxicity toward the cells, but the cell viability of each treatment group was still more than 60 %. Only **A2** and **A10** were two most toxic compounds, but results in a considerably higher survival rate than the PL-treatment group.

Hydrogen peroxide (H_2O_2) is an uncharged redox sensing and redox signaling molecule, and can generate highly reactive free radicals immediately, which is able to

cause deleterious effects to lipid, proteins and nucleic acid, and ultimately lead to many pathophysiological conditions [30]. Therefore, the cytoprotection against the H_2O_2-induced oxidative damage in PC12 cells was evaluated for the PL analogs. As shown in Figure 2B, the survival rate of PC12 cells treated with H_2O_2 was about half of the control group (DMSO). However, when the cells were pretreated by the tested compounds for 24 h prior to H_2O_2 insult, 24 compounds (10 μM) improved the survival rate to 70-80%, of which about half provided more protection than compound **a**. Among these compounds, **A3**, **A5**, **A7**, **A9**, **A11**, **A18**, **A21** and **A23** showed the same efficient antioxidant effect as TBHQ (tert-butylhydroquinone, a Nrf2 activator). In contrast, compounds **A2**, **A10**, **A13**, **A14**, **A27** and **A28** could not significantly protect PC12 cells from H_2O_2-induced cell injury, which might relate to their toxic effects. PL showed no protective effect in this assay. Besides, compounds **A15**, **A16** and **A17** also could not greatly reduce the cell injury because of the low cytotoxicity. Taken together, as long as the analogs are not toxic or less toxic, they can display cytoprotection activity.

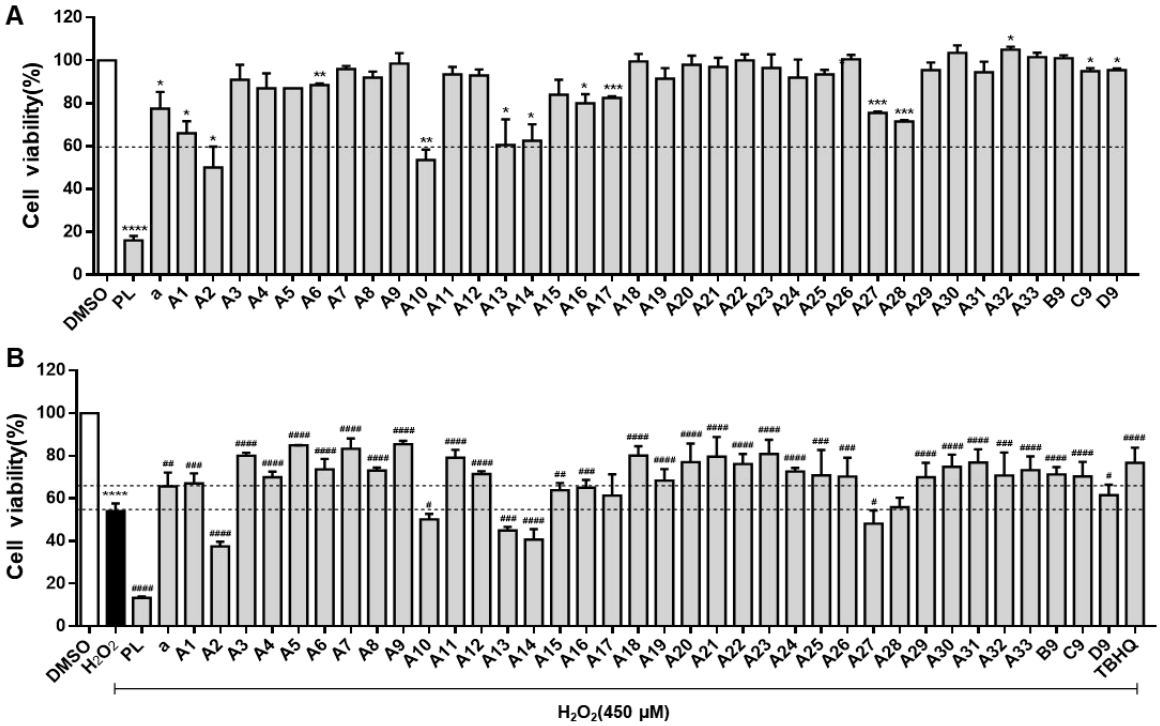

Figure 2. The cytotoxicity screening and cytoprotection of compounds in PC12 cells. (A) Cells were plated in 96-well plates for 24 h and subsequently treated with 10 μM compounds for 24 h. The cell viability was determined by the MTT assay. (B) PC12 cells were pretreated with the compounds for 24 h (10 μM), and then exposed to H_2O_2 (450 μM) for another 24 h. The effect of compounds on cell viability measured by MTT assay and the viability of untreated cells is defined as 100%. Data are expressed as the mean ± SD, n = 3. $^{****}p < 0.0001$, $^{***}p < 0.001$, $^{**}p < 0.01$, $^{*}p < 0.05$ vs DMSO, $^{\#\#\#\#}p < 0.0001$, $^{\#\#\#}p < 0.001$, $^{\#\#}p < 0.01$, $^{\#}p < 0.05$ vs H_2O_2.

To get insight in the SAR and to evaluate the effects of various substituents on the

bioactivity, the SAR of 33 analogs was further analyzed. Interesting, results showed that analogs [**A4** (4-methoxy), **A12** (2-methoxy) **A11** (2,4-dimethoxy) and **A9** (2,4,6-trimethoxy)] with increasing number of methoxy substitutions on phenyl ring showed enhanced cytoprotection. Additionally, the similar phenomenon occurred in analogs [**A32** (3-methoxy), **A24** (3,4-dimethoxy) **A33** (3,5-dimethoxy) and **A23** (3,4,5-trimethoxy)]. It was found that except **A15** (2,3-dimethoxy) with high level of toxicity cytotoxicity, the same sort of phenomenon was observed among **A12** (2-methoxy), **A11** (2,4-dimethoxy) and **A18** (2,5-dimethoxy). Nevertheless, there is opposite phenomenon in the benzene ring with hydroxy moiety. The analogs with one hydroxyl group [**A6** (4-hydroxy) or **A7** (3-hydroxy)] exhibited stronger antioxidant activity than that containing two hydroxyl groups [**A17** (3,4-dihydroxy)]. Furthermore, compared with electron withdrawing group at 4-position [compounds **A20** (4-Cl) and **A30** (4-Br)], analogs with electron withdrawing group at 2-position [**A16** (2-CF3) and **A19** (2-Br)] displayed weaker cytoprotection. In summary, the substitution of methoxy group can reinforce the protective effect, and the position of electron-withdrawing substitution on a ring could affect the activity, respectively.

To explore the importance of 3,4,5-trimethoxy and olefinic double bonds, the most active compound **A9** was selected for structural modification. As shown in Figure 2B, the 3,4,5-tridemethoxy derivative (**B9**), showed weaker cytoprotective activity compared with **A9**. In the meanwhile, compounds **1** and **2**, two reduction products of the carbon-carbon double bonds in **A9**, also exhibited weaker protection in comparison with **A9**. These results further confirmed that the double bonds of Michael acceptor and 3,4,5-trimethoxy (highlighted in Figure 3) may be essential to strengthen the protective effect.

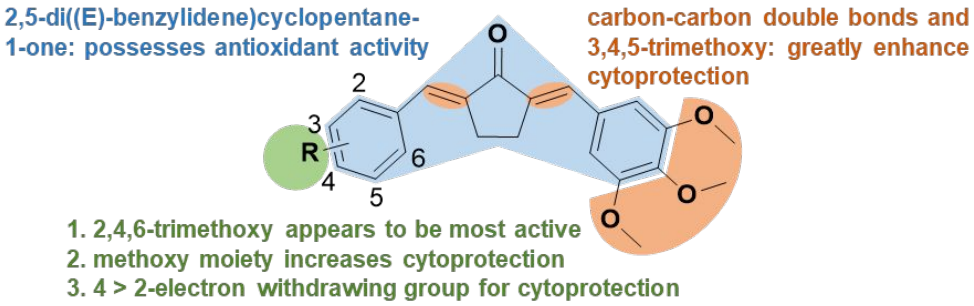

Figure 3. SAR analysis of PL analogs

2.3 Protective effect of A9 in different cellular injury models

A9 was selected for further studies owing to its the better protection and lower toxicity. Besides H_2O_2-induced PC12 cell damage model, the other three cellular models including glutamate-, glucose- and LPS-induced cellular PC12 cell damage model were employed for

further evaluating the antioxidant effect of **A9** in vitro. The proper concentrations of the glutamate, glucose or LPS were determined under the guidance of literature material [31-33]. As shown in Figure 4, when the cells were treated with **A9** for 24 h prior to different insults, the cell viabilities were increased in a dose-dependent manner in each model.

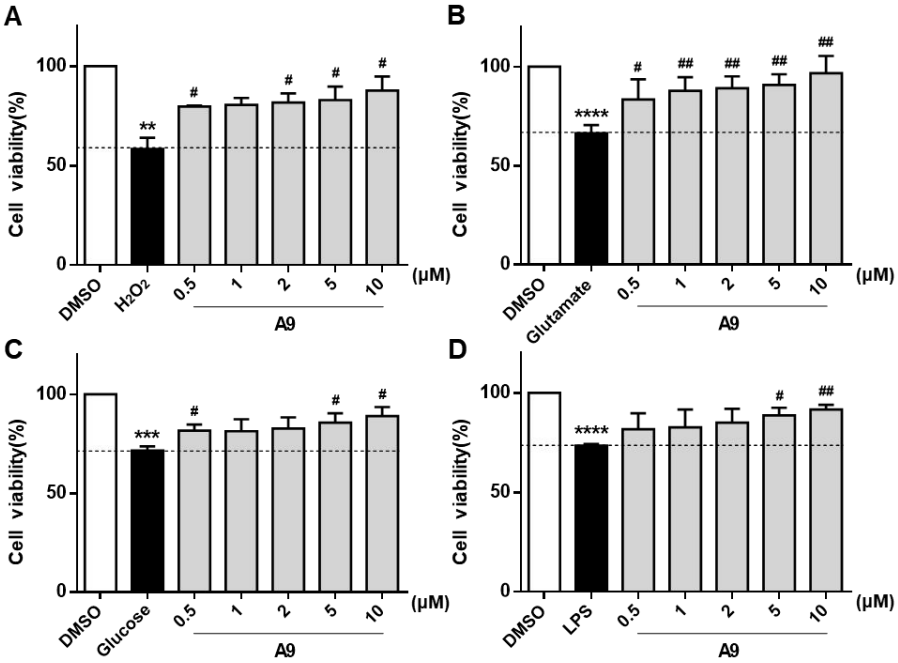

Figure 4. A9 Protects PC12 Cells in different cellular injury model. Cells were preincubated with different concentrations of **A9** for 24 h before treatment with 450 μM H_2O_2 (A), 18 mM glutamate (B), 45 μg/ml LPS (D) for 24 h or 140 mM glucose (C) for 48 h. The survival cells were determined by MTT assay and the viability of untreated cells is defined as 100%. Data are expressed as the mean ± SD, n = 3. ****$p < 0.0001$, **$p < 0.01$vs DMSO, $^{\#\#}p < 0.01$, $^{\#}p < 0.05$ vs H_2O_2.

2.4 The cytoprotection of A9 in rat primary astrocytes and cortical neurons

Since **A9** was verified to have significant cytoprotective effect, its antioxidant activity was further investigated in rat primary cells. It is crucial that astrocytes provide antioxidants and support the survival of neurons in the central nervous system [34-35]. Therefore, the cytoprotection against H_2O_2-induced rat primary astrocytes and cortical neurons cell damage was evaluated for **A9**. As shown in Figure 5, after treatment with **A9** for 24 h prior to H_2O_2 insult, the population of viable cells was increased remarkably.

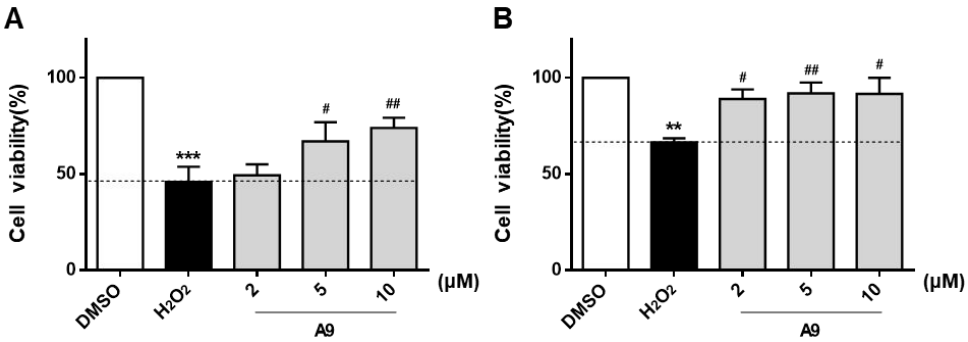

Figure 5. A9 protected rat primary astrocytes (A) and cortical neurons (B) from H_2O_2-induced cell injury in a dose-dependent manner. The cell viability was determined by the MTT assay. Data are expressed as the mean ± SD, n = 3. ***$p < 0.001$, **$p < 0.01$vs DMSO, ##$p < 0.01$, #$p < 0.05$ vs H_2O_2.

2.5 The antioxidative protection of A9 against H_2O_2-induced oxidative stress injury

The antioxidant activity of **A9** (2 μM) against H_2O_2-induced oxidative damage was further studied. **A9** promoted colony formation of PC12 cells in H_2O_2-induced oxidative damage model (Figure 6A). The apoptosis rate increased after treatment with H_2O_2, but **A9** resisted H_2O_2-induced apoptosis in PC12 cells (Figure 6B). ROS can induce the excessive accumulation of malondialdehyde (MDA), lactate dehydrogenase (LDH) and so on. The level of intracellular ROS was elevated by H_2O_2, and **A9** significantly suppressed the formation of ROS (Figure 6C). In addition, as shown in Figure 6D, the level of MDA in the **A9** group was dramatically lower than that in the control group, suggesting that **A9** blocked MDA accumulation in PC12 cells, and the treatment of cells with H_2O_2 led to LDH release, which was significantly decreased by a post-treatment of the cells with **A9** (Figure 6E). Above all, **A9** protected PC12 cells from H_2O_2-induced cell injury by inhibiting cell apoptosis, scavenging ROS, decreasing LDH release and reducing MDA.

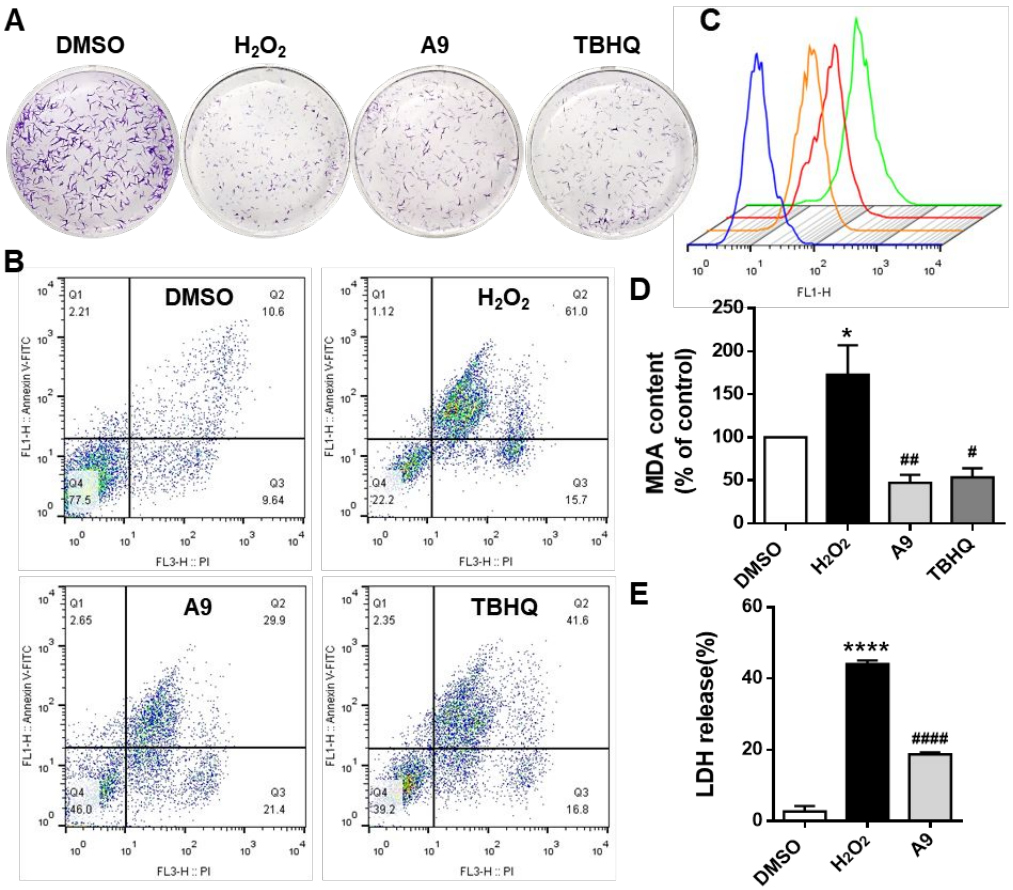

Figure 6. The antioxidant effects of **A9** (2 μM) against H_2O_2-induced oxidative damage in PC12 cells. (A) **A9** promoted colony formation of PC12 cells in H_2O_2 damage model. Cells were incubated by **A9** for 24 h, and then incubation with 100 μM H_2O_2 for 6 days. Representative photographs of the colony

formation assay. (B, C, D) PC12 cells were incubated with **A9** for 24 h before exposure in H_2O_2 (1 mM) for 6 h (B, D) or 2h (C). The rate of cell apoptosis (B), the level of intracellular ROS (C) and the MDA levels (D) were determined according to the manufacturer's instructions. (E) Effect of **A9** on the LDH release from PC12 cells after 450 μM H_2O_2 treatment for 24 h. TBHQ (2 μM) was used as the positive control. Data are expressed as the mean ± SD, n = 3. ****$p < 0.0001$, *$p < 0.05$ vs DMSO, ####$p < 0.001$, ##$p < 0.01$, #$p < 0.05$ vs H_2O_2.

2.6 The antioxidant effect of A9 by activating Nrf2 signaling pathway

The Nrf2 (nuclear factor erythroid 2-related factor 2) transcription factor plays a critical role in cellular oxidative stress response [36-38]. Hence, to investigated whether the antioxidant effect of **A9** is dependent on the activation of Nrf2 signaling pathway, Nrf2 siRNA or control siRNA was transfected into PC12 cells using Lipofectamine 2000 reagent, and the cytoprotective effects of **A9** against oxidative stress injury toward different cells were evaluated. The results indicated that down-regulation of Nrf2 expression dramatically decreased the cytoprotective effect of **A9** (Figure 7A and B). Besides, **A9** enhanced the expression of HO-1 (heme oxygenase-1) protein, while its cytoprotection was reversed by the HO-1 protein inhibitor ZnPP [39] (Figure 7C and D). Over all, **A9** can activate the Nrf2 signaling pathway to protect PC12 cells against H_2O_2-derived oxidative cell death.

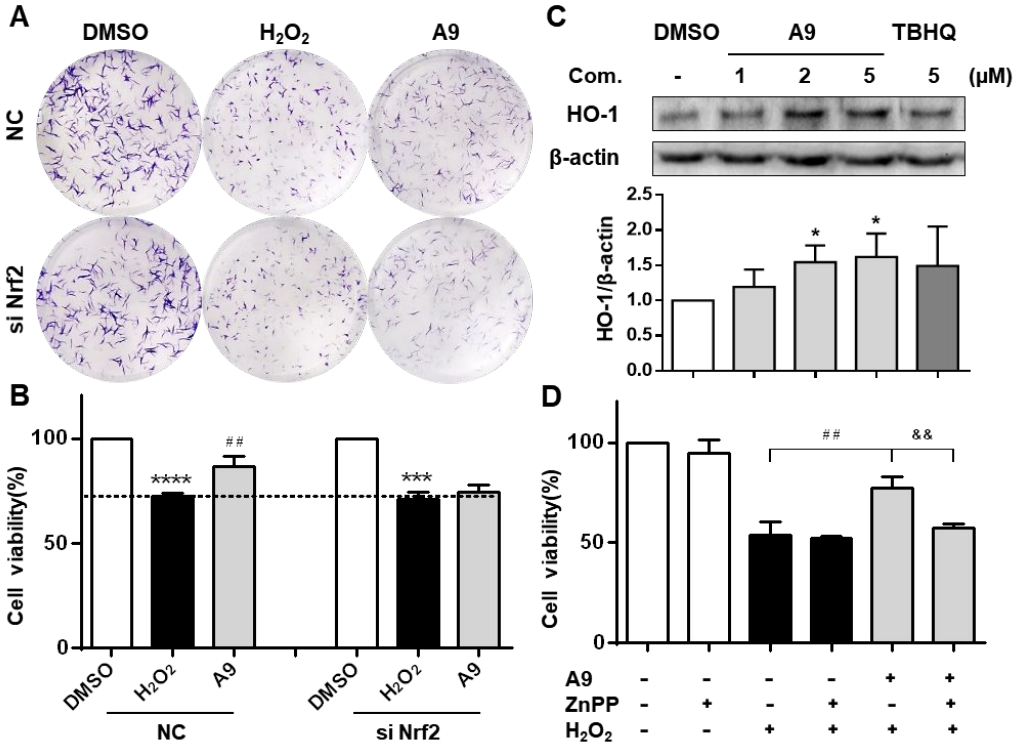

Figure 7. A9 protects PC12 cells from H_2O_2-induced cell injury by activating Nrf2 signaling pathway. (A, B) Down-regulation of Nrf2 expression by siRNA diminished the protective effect of **A9** on H_2O_2 induced cell damage. PC12 cells were transfected with si Nrf2 or negative control siRNA (NC) for 48 h and the transfected cells were collected. The cells were pretreated with 2 μM **A9** followed by H_2O_2 treatment for 24 h. The survival cells were represented by the colony formation assay and determined by

MTT assay. (C) **A9** increased the levels of HO-1 protein. PC12 cells were incubated with **A9** (1, 2 and 5 μM) for 24 h. Next, the proteins were extracted and analyzed by western blot assay. (D) HO-1 inhibitor ZnPP decreased the protection of **A9** in H_2O_2 damage model. PC12 cells were pretreated with ZnPP for 1 h, and then treated with the 2 μM **A9** for 24 h followed by another 24 h H_2O_2 (450 μM) exposure. TBHQ was used as the positive control. Data are expressed as the mean ± SD, n = 3. ****$p < 0.0001$, ***$p < 0.001$, *$p < 0.05$ vs DMSO, ##$p < 0.01$ vs H_2O_2, &&$p < 0.01$.

2.7 Preventative therapies of A9 against CIRI

Transient transcranial middle cerebral artery occlusion (MCAO) model is a common method to evaluate ischemic stroke in vivo [40-41]. The neuroprotective effect of **A9** was further investigated using a MCAO model. At 72 h after reperfusion, the neurological deficit was evaluated on the basis of neurologic score and the infarct area was measuring using TTC staining. The treatment with **A9** showed a protective effect on infarction damage (Figure 8). Pre-treatment of **A9** reduced not only the infracted brain areas but also corresponding neurological score.

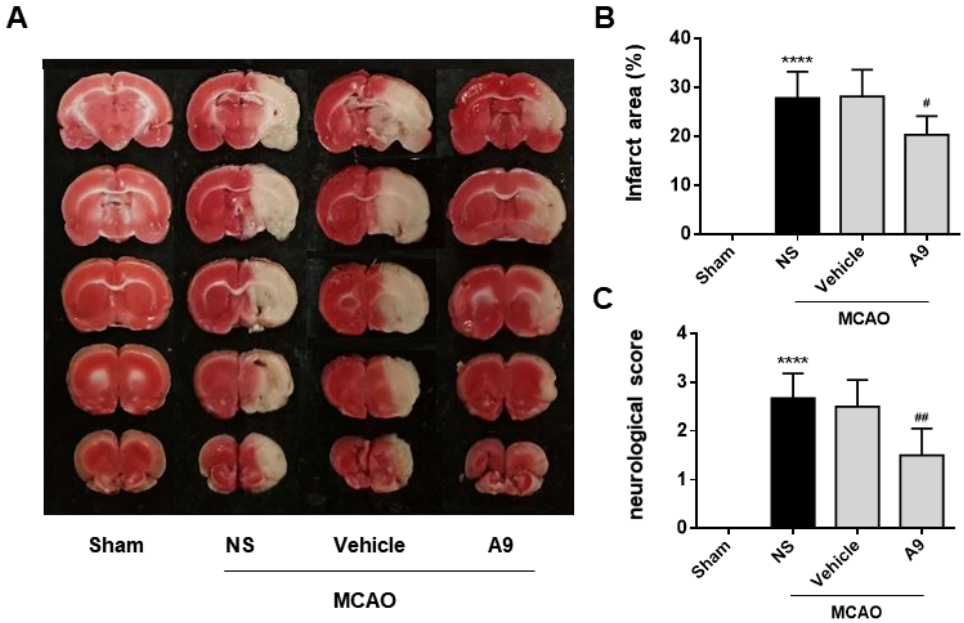

Figure 8. Protective effect of **A9** after MCAO in rats. (A) Representative photographs of brain slices with TTC staining of each group. (B) Quantitative analysis of the infracted brain regions. (C) The corresponding neurological score levels in brain tissues. Cerebral infarction in sham-operated (sham) or MACO reperfusion rats from a representative animal that received normal saline (NS), vehicle (the ratio of DMSO and NS was 1:100) and 0.15 mg/kg **A9** by intraventricular injection. Data are expressed as the mean ± SD, n = 6. ****$p < 0.0001$ vs sham-operated group, ##$p < 0.01$, #$p < 0.05$ vs vehicle-treated group.

3. DISCUSSION

Natural products play an important part in the discovery of small molecule drugs, and more and more attention has been paid to the biological functions of PL extracted from long pepper [42-44]. In this study, a series of new PL analogs have been synthesized, and a

potent compound with the neuroprotective effects against CIRI was identified.

PL can cause a prominent toxic effect on nerve cells, though, it has wide prospects of application as neuroprotective agent. To minimize the cytotoxicity of PL, we have introduced a diketene structure based on the diketene skeletons of cytoprotective agents. Although these agents (shown in Figure 1B) have different diketene skeletons, all of them can protect the tissue or cells from damage. For example, compound B82 derived from acetone demonstrated cytoprotection abilities in a dose-dependent manner [17]. The piperid-4-one- containing F36 dose-dependently prevented NF-κB and ERK activation in the cells and attenuated the septic death in mice [18]. The new MD2 specific inhibitor L48H37 whose central linker is a N-ethyl-4-piperidin-4-one significantly improved survival and protected lung injury in mice [19]. Pyranone-derived compound MAC 17 effectively inhibited the LPS-stimulated cytokine secretion from macrophages, and protected against acute lung injury and sepsis [20]. Then we discovered that the activity and toxicity of the diketene skeletons may be related to the different type of intermediate join ketone. We conducted subsequent studies to examine the various diketene skeletons and later discovered 2,5-di((E)-benzylidene) cyclopentan-1-one (skeleton a) with low toxicity and antioxidant ability.

To investigate the effects of 3,4,5-trimethoxybenzyl and α,β-unsaturated ketone structures on the antioxidant activity of PL, we used the selected skeleton **a** to combine with the 3,4,5-trimethoxyphenyl group of PL to obtain a series of PL analogs, namely 2-((E)-substituted benzylidene)-5-((E)-3,4,5-trimethoxybenzylidene)cyclopentan-1-one analogs. To gain insight into the structure-activity relationship of the synthesized PL analogs, the toxicity and activity of a number of compounds were tested. The results showed that any the synthesized PL analogs without obvious cytotoxicity have better antioxidant function than the diketene skeleton and PL. When the 3,4,5-trimethoxy group was remove from the structure of the optimal compound **A9**, its activity was greatly reduced, suggesting that the 3,4,5-trimethoxy moiety in the benzene ring in PL could increase the antioxidative effect. In addition, the cell viability also notably decreased when the carbon-carbon double bonds of **A9** were reduced by hydrogen, indicating that the diketene skeleton of PL analogs is important for the ability of antioxidation. In short, it was concluded that the methoxy groups and olefinic double bonds of PL analogs may be critical for its neuroprotective effects.

The pathophysiological mechanism of CIRI is quite complicated, which includes oxidative stress, glutamate excitotoxicity, inflammation and so on [45-47]. In this study, four cellular models (H_2O_2-, glucose-, glutamate- and LPS-induced damage models) were

selected to study the antioxidative protection of the optimal compound **A9**. As a result, it was found that the active compound **A9** could dose-dependently enhance the cell viability in each damage model. Subsequently, the cytoprotective antioxidant effect of **A9** was confirmed in rat primary astrocytes. In addition, **A9** was identified as a potent Nrf2 activator, which could reduce the levels of intracellular ROS and MDA, and inhibit LDH release and apoptosis to protect cells from oxidative damage. More interestingly, **A9** showed a favorable neuroprotection against ischemic brain injury.

4. CONCLUSIONS

In summary, a series of new PL analogs were designed by the combination of active diketene skeleton and the 3,4,5-trimethoxybenzyl moiety which could enhance the antioxidant property of PL. The synthesis was accomplished by a green synthetic method of taking L-proline as a catalyst for one-step synthesis of intermediates. The vast majority of PL analogs obtained exhibited stronger antioxidant activity than the diketene skeleton (skeleton **a**), and the most active compound **A9** was revealed to be an effective Nrf2 activator with lower cytotoxicity. **A9** can not only activate the Nrf2-dependent cytoprotective pathway and up-regulate the expression of antioxidant proteins, but also remarkably reduce the infarcted brain areas of rats subjected to CIRI. Taken together, the PL analogs obtained by a green synthetic strategy demonstrated neuroprotective antioxidant effects and might have the potential to treat brain disorders. **A9** as a promising anti-CIRI lead compound, its targets and underlying molecular mechanism remain to be clarified.

5. Experimental Section

5.1 General

Commercially available starting materials and reagents were purchased from Sigma-Aldrich (St Louis, Missouri, USA), Aladdin (Shanghai, China) and used without further purification. All reactions were monitored by thin-layer chromatography TLC using silica gel GF254. The chromatograms were conducted on silica gel (200-300 mesh) and observed under UV light at 254 and 365 nm. Moreover, melting points (Mp) were determined in open capillary tubes on a Fisher-Johns melting apparatus and uncorrected. Mass spectra (MS) were recorded at the Agilent 1100 LC-MS (Agilent, Palo Alto, CA, USA). ^{1}H NMR spectra were acquired on a 500 or 600 MHz spectrometer (Bruker Corporation, Switzerland) using $CDCl_3$ or DMSO-d_6 as solvent. Tetramethylsilane (TMS) was used as the internal standard. Coupling constants (J) are expressed in Hz, and splitting

patterns are described as follows: s = singlet; d = doublet; t = triplet; m = multiplet; dd = doublet of doublets; dt = doublet of triplets.

5.2 Synthetic procedures

5.2.1 General synthetic procedure for the synthesis of intermediate

3,4,5-trimethoxybenzaldehyde (0.196 g, 1.0 mmol, 1.0 equiv.), cyclopentanone (0.421 g, 5.0 mmol, 5.0 equiv.) and L-proline (0.23 g, 0.2 mmol, 0.2 equiv.) were dissolved in anhydrous dimethylsulfoxide (2 mL) and the mixture was stirred for 24 h at room temperature. Then, add 5 drops concentrated hydrochloric acid was added to the solution and continuously stirred for 2 h at room temperature. The completion of the reaction was monitored using TLC analysis. When the starting material was completely consumed, H_2O (10 mL) was added to the reacted mixture and extracted by ethyl acetate (15 mL, 3 times). The organic layer was dried with anhydrous $MgSO_4$, concentrated and evaporated in vacuo. Finally, the crude product was purified by silica gel chromatography. Ethyl acetate and petroleum ether were used as mobile phases.

5.2.2 General synthetic procedure for the synthesis of A and B series compounds

A mixture of the intermediate (0.26 g, 1.0 mmol, 1.0 equiv.) and the corresponding aldehyde (1.2 mmol, 1.2 equiv.) in anhydrous EtOH was stirred at room temperature for 5 min. Then NaOH or HCl (gas) was added into the solution as catalyst to accelerate the reaction. The reaction mixture was stirred at room temperature until raw material was totally consumed (usually 6-12 h). Completion of the reaction was monitored by thin layer chromatography using ethyl acetate/hexanes as the solvent system. After the reaction completed, the crude product was filtered out and crystallized with hot ethanol or purified by using silica gel chromatography.

5.2.3 General synthetic procedure for the synthesis of 1 and 2

A9 (0.44 g, 1.0 mmol, 1.0 equiv.) was dissolved in ethanol-ethyl acetate (5 mL/1mL), and 10% palladium on charocoal was stirred under hydrogen for 12 h or 24 h at room temperature. The catalyst was removed by filtration and the solvent was evaporated. The residue was purified on a silica gel column using petroleum ether/ethyl acetate as eluent to yield the **1** or **2** as colourless oil.

The spectral data of compounds are listed as follows:

2-((E)-2,4-dichlorobenzylidene)-5-((E)-3,4,5-trimethoxybenzylidene)cyclopentan-1-one (A1): Yellow power, 61.9% yield, mp 202.3~203.5 °C. ^{1}H-NMR (600 MHz, *d*-DMSO), δ: 7.846 (s, 1H, β-H), 7.555-7.501 (m, 3H, Ar-H$^{3'}$, Ar-H$^{5'}$, Ar-H$^{6'}$), 7.325 (d,

J=7.2 Hz, 1H, α-H), 6.852 (s, 2H, Ar-H^2, Ar-H^6), 3.931 (s, 9H, 3-OCH_3, 5-OCH_3, 4-OCH_3), 3.125 (s, 2H, CH_2), 3.031 (s, 2H, CH_2). LC-MS m/z: 419.17 $(M+H)^+$, calcd for $C_{22}H_{20}Cl_2O_4$: 418.07.

2-((E)-4-(dimethylamino)benzylidene)-5-((E)-3,4,5-trimethoxybenzylidene)cyclopentan-1-one (A2): Orange power, 65.6% yield, mp 201.3~202.4 °C. ^{1}H-NMR (600 MHz, *d*-DMSO), δ: 7.604 (s, 1H, β-H), 7.557 (d, *J*=8.4 Hz, 2H, Ar-$H^{6'}$, Ar-$H^{2'}$), 7.448 (s, 1H, α-H), 6.868 (s, 2H, Ar-H^2, Ar-H^6), 6.757 (d, *J*=9.0 Hz, 2H, Ar-$H^{3'}$, Ar-$H^{5'}$), 6.930 (d, *J*=6.6 Hz, 9H, 3-OCH_3, 5-OCH_3, 4-OCH_3), 3.118 (s, 4H, CH_2CH_2), 3.070 (s, 6H, CH_3NCH_3). LC-MS m/z: 394.05 $(M+H)^+$, calcd for $C_{24}H_{27}NO_4$: 393.19.

2-((E)-4-hydroxy-3-methoxybenzylidene)-5-((E)-3,4,5-trimethoxybenzylidene)cyclopentan-1-one (A3): Orange power, 68.6% yield, mp 114.8~115.5 °C. ^{1}H-NMR (600 MHz, *d*-DMSO), δ: 9.703 (s, 1H, 4'-OH), 7.371 (dt, *J*=9.6 Hz, *J*=10.2 Hz, 2H, β-H, α-H), 7.245 (d, *J*=1.8 Hz, 1H, Ar-$H^{6'}$), 7.157 (dd, *J*=1.8 Hz, *J*=8.4 Hz, 1H, Ar-$H^{2'}$), 6.983 (s, 2H, Ar-H^2, Ar-H^6), 6.878 (d, *J*=8.4 Hz, 1H, Ar-$H^{5'}$), 3.827 (d, *J*=1.8 Hz, 9H, 3-OCH_3, 5-OCH_3, 3'-OCH_3), 3.702 (s, 3H, 4-OCH_3), 3.129-3.111 (m, 2H, CH_2), 3.076-3.052 (m, 2H, CH_2). LC-MS m/z: 396.16 $(M+H)^+$, calcd for $C_{23}H_{24}O_6$: 397.17.

2-((E)-4-methoxybenzylidene)-5-((E)-3,4,5-trimethoxybenzylidene)cyclopentan-1-one (A4): Yellow power, 69.8% yield, mp 186.5~189.2 °C. ^{1}H-NMR (600 MHz, $CDCl_3$), δ: 7.594 (d, *J*=8.4 Hz, 2H, Ar-$H^{2'}$, Ar-$H^{6'}$), 7.553 (t, *J*=4.2 Hz, 1H, β-H), 7.525 (s, 1H, α-H), 7.000 (d, *J*=9.0 Hz, 2H, Ar-$H^{3'}$, Ar-$H^{5'}$), 6.870 (s, 2H, Ar-H^2, Ar-H^6), 3.933 (d, *J*=5.4 Hz, 9H, 3-OCH_3, 5-OCH_3, 4'-OCH_3), 3.886 (s, 3H, 4-OCH_3), 3.153-3.113 (m, 4H, CH_2CH_2). LC-MS m/z: 381.16 $(M+H)^+$, calcd for $C_{23}H_{24}O_5$: 380.16.

2-((E)-2-hydroxybenzylidene)-5-((E)-3,4,5-trimethoxybenzylidene)cyclopentan-1-one (A5): Yellow power, 68.7% yield, mp 123.6~125.9 °C. ^{1}H-NMR (600 MHz, $CDCl_3$), δ: 9.904 (s, 1H, 2'-OH), 7.530 (s, 1H, β-H), 7.317 (t, *J*=2.4 Hz, 2H, α-H, Ar-$H^{6'}$), 6.855 (s, 3H, Ar-H^2, Ar-H^6, Ar-$H^{5'}$), 6.713 (s, 1H, Ar-$H^{4'}$), 6.642 (s, 1H, Ar-$H^{3'}$), 3.893 (s, 9H, 3-OCH_3, 4-OCH_3, 5-OCH_3), 3.150 (s, 2H, CH_2), 3.012-2.984 (m, 2H, CH_2). LC-MS m/z: 367.26 $(M+H)^+$, calcd for $C_{22}H_{22}O_5$: 366.15.

3-((E)-4-hydroxybenzylidene)-5-((E)-3,4,5-trimethoxybenzylidene)cyclopentan-1-one (A6): Brown power, 77.3% yield, mp 232.5~233.1 °C. ^{1}H-NMR (600 MHz, *d*-DMSO), δ: 10.104 (s, 1H, 4'-OH), 7.558 (d, *J*=8.4 Hz, 2H, Ar-$H^{2'}$, Ar-$H^{6'}$), 7.384 (d, *J*=2.4 Hz, 2H, β-H, α-H), 7.033 (s, 2H, Ar-H^2, Ar-H^6), 6.891 (d, *J*=8.4 Hz, 2H, Ar-$H^{3'}$, Ar-$H^{5'}$), 3.850 (s, 6H, 3-OCH_3, 5-OCH_3), 3.723 (s, 3H, 4-OCH_3), 3.138-3.123 (m, 2H, CH_2), 3.048-3.033 (m, 2H, CH_2). LC-MS m/z: 367.15 $(M+H)^+$, calcd for $C_{22}H_{22}O_5$: 366.15.

2-((E)-3-hydroxybenzylidene)-5-((E)-3,4,5-trimethoxybenzylidene)cyclopentan-1-one (A7): Yellow power, 78.9% yield, mp 123.6~125.9 °C. ^{1}H-NMR (600 MHz, *d*-DMSO), δ: 9.639 (s, 1H, 3'-OH), 7.401 (s, 1H, β-H), 7.324 (s, 1H, α-H), 7.273 (t, *J*=7.8 Hz, 1H, Ar-$H^{5'}$), 7.096 (d, *J*=7.2 Hz, 1H, Ar-$H^{6'}$), 7.061 (s, 1H, Ar-$H^{4'}$), 6.996 (s, 2H, Ar-H^2,

Ar-H^6), 6.836-6.821 (m, 1H, Ar-H$^{2'}$), 3.831 (s, 6H, 3-OCH$_3$, 5-OCH$_3$), 3.705 (s, 3H, 4-OCH$_3$), 3.126 (d, *J*=6.0 Hz, 2H, CH$_2$), 3.050 (d, *J*=5.4 Hz, 2H, CH$_2$). LC-MS m/z: 367.26 (M+H)$^+$, calcd for $C_{22}H_{22}O_5$: 366.15.

2-((E)-3-fluorobenzylidene)-5-((E)-3,4,5-trimethoxybenzylidene)cyclopentan-1-one (A8): Yellow power, 69.9% yield, mp 140.4~141.5 °C. ^{1}H-NMR (600 MHz, CDCl$_3$), δ: 7.555 (s, 3H, β-H, α-H, Ar-H$^{6'}$), 7.447-7.410 (m, 2H, Ar-H$^{5'}$, Ar-H$^{4'}$), 7.105 (td, *J*=1.2 Hz, *J*=7.2 Hz, 1H, Ar-H$^{2'}$), 6.868 (s, 2H, Ar-H^2, Ar-H^6), 3.934 (d, *J*=2.4 Hz, 9H, 3-OCH$_3$, 5-OCH$_3$, 4-OCH$_3$), 3.148 (s, 4H, CH$_2$CH$_2$). LC-MS m/z: 369.11 (M+H)$^+$, calcd for $C_{22}H_{21}FO_4$: 368.14.

2-((E)-2,4,6-trimethoxybenzylidene)-5-((E)-3,4,5-trimethoxybenzylidene)cyclopentan-1-one (A9): Yellow power, 72.3% yield, mp 163.3~164.0 °C. ^{1}H-NMR (600 MHz, CDCl$_3$), δ: 7.698 (s, 1H, β-H), 7.475 (s, 1H, α-H), 6.851 (s, 2H, Ar-H^2, Ar-H^6), 6.178 (s, 2H, Ar-H$^{3'}$, Ar-H$^{5'}$), 3.921 (s, 6H, 2'-OCH$_3$, 6'-OCH$_3$), 3.860 (s, 9H, 3-OCH$_3$, 5-OCH$_3$, 4'-OCH$_3$), 3.806 (s, 3H, 4-OCH$_3$), 3.055-2.988 (m, 4H, CH$_2$CH$_2$). LC-MS m/z: 441.24 (M+H)$^+$, calcd for $C_{25}H_{28}O_7$: 440.18.

2-((E)-3-hydroxy-4-methoxybenzylidene)-5-((E)-3,4,5-trimethoxybenzylidene)cyclopentan-1-one (A10): Yellow power, 73.8% yield, mp 190.1~191.3 °C. ^{1}H-NMR (600 MHz, *d*-DMSO), δ: 9.299 (s, 1H, 3'-OH), 7.388 (s, 1H, β-H), 7.325 (s, 1H, α-H), 7.148 (d, *J*=7.2 Hz, 2H, Ar-H$^{2'}$, Ar-H$^{6'}$), 7.042 (d, *J*=9.0 Hz, 1H, Ar-H$^{5'}$), 7.006 (s, 2H, Ar-H^2, Ar-H^6), 3.852 (s, 6H, 3-OCH$_3$, 5-OCH$_3$), 3.836 (s, 3H, 4'-OCH$_3$), 3.724 (s, 3H, 4-OCH$_3$), 3.146-3.135 (m, 2H, CH$_2$), 3.039-3.029 (m, 2H, CH$_2$). LC-MS m/z: 397.23 (M+H)$^+$, calcd for $C_{23}H_{24}O_6$: 396.16.

2-((E)-2,4-dimethoxybenzylidene)-5-((E)-3,4,5-trimethoxybenzylidene)cyclopentan-1-one (A11): Yellow power, 68.2% yield, mp 164.0~165.8 °C. ^{1}H-NMR (600 MHz, CDCl$_3$), δ: 8.027 (s, 1H, Ar-H$^{6'}$), 7.541 (d, *J*=8.4 Hz, 1H, β-H), 7.509 (s, 1H, α-H), 6.862 (s, 2H, Ar-H^2, Ar-H^6), 6.584-6.506 (m, 2H, Ar-H$^{3'}$, Ar-H$^{5'}$), 3.933-3.914 (m, 12H, 2'-OCH$_3$, 4'-OCH$_3$, 3-OCH$_3$, 5-OCH$_3$), 3.900 (s, 3H, 4-OCH$_3$), 3.118-3.060 (m, 4H, CH$_2$CH$_2$). LC-MS m/z: 411.15 (M+H)$^+$, calcd for $C_{24}H_{26}O_6$: 410.17.

2-((E)-2-methoxybenzylidene)-5-((E)-3,4,5-trimethoxybenzylidene)cyclopentan-1-one (A12): Yellow power, 71.3% yield, mp 117.2~118.3 °C. ^{1}H-NMR (600 MHz, CDCl$_3$), δ: 8.046 (s, 1H, Ar-H$^{4'}$), 7.558 (t, *J*=7.2 Hz, 2H, β-H, Ar-H$^{6'}$), 7.401-7.374 (m, 1H, α-H), 7.032 (t, *J*=7.8 Hz, 1H, Ar-H$^{3'}$), 6.968 (d, *J*=7.8 Hz, 1H, Ar-H$^{5'}$), 6.866 (s, 2H, Ar-H^2, Ar-H^6), 3.935 (s, 6H, 3-OCH$_3$, 5-OCH$_3$), 3.927 (s, 3H, 2'-OCH$_3$), 3.918 (s, 3H, 4-OCH$_3$), 3.104 (s, 4H, CH$_2$CH$_2$). LC-MS m/z: 381.16 (M+H)$^+$, calcd for $C_{23}H_{24}O_5$: 380.16.

2-((E)-4-(piperidin-1-yl)benzylidene)-5-((E)-3,4,5-trimethoxybenzylidene)cyclopentan-1-one (A13): Orange powder, 64.8% yield, mp 171.2~171.7 °C. ^{1}H-NMR (600 MHz, CDCl$_3$), δ: 7.585 (s, 1H, Ar-H$^{2'}$), 7.542 (d, *J*=9.0 Hz, 2H, β-H, α-H), 7.497 (s, 1H, Ar-H$^{6'}$), 6.948 (d, *J*=9.0 Hz, 2H, Ar-H$^{3'}$, Ar-H$^{5'}$), 6.869 (s, 2H, Ar-H^2, Ar-H^6), 3.930 (d, *J*=6.6 Hz,

9H, 3-OCH_3, 5-OCH_3, 4-OCH_3), 3.349 (t, *J*=10.2 Hz, 4H, CH_2NCH_2), 3.123 (s, 4H, CH_2CH_2), 0.901 (t, *J*=7.8 Hz, 6H, $CH_2CH_2CH_2$). LC-MS m/z: 433.96 $(M+H)^+$, calcd for $C_{27}H_{31}NO_4$: 433.23.

2-((E)-4-morpholinobenzylidene)-5-((E)-3,4,5-trimethoxybenzylidene)cyclopentan-1-one (A14): Orange powder, 56.4% yield, mp 191.4~192.5 °C. ^{1}H-NMR (600 MHz, $CDCl_3$), δ: 7.563 (d, *J*=9.0 Hz, 2H, Ar-$H^{2'}$, Ar-$H^{6'}$), 7.531 (d, *J*=7.2 Hz, 4H, β-H, α-H, Ar-H^2, Ar-H^6), 7.404-7.318 (m, 8H, Ar-$H^{3'}$, Ar-$H^{5'}$, 3-OCH_3, 5-OCH_3), 7.009 (t, *J*=6.9 Hz, 4H, CH_2OCH_2), 6.947 (d, *J*=9.0 Hz, 3H, 4-OCH_3), 3.891 (t, *J*=4.8 Hz, 4H, CH_2NCH_2), 3.295 (t, *J*=4.8 Hz, 4H, CH_2CH_2). LC-MS m/z: 436.20 $(M+H)^+$, calcd for $C_{26}H_{29}NO_5$: 435.20.

2-((E)-2,3-dimethoxybenzylidene)-5-((E)-3,4,5-trimethoxybenzylidene)cyclopentan-1-one (A15): Yellow powder, 58.6% yield, mp 150.5~151.3 °C. ^{1}H-NMR (600 MHz, $CDCl_3$), δ: 7.957 (s, 1H, β-H), 7.545 (d, *J*=1.2 Hz, 1H, α-H), 7.196 (d, *J*=7.2 Hz, 1H, Ar-$H^{6'}$), 7.134 (t, *J*=16.2 Hz, 1H, Ar-$H^{5'}$), 6.997-6.946 (m, 1H, Ar-$H^{4'}$), 6.867 (s, 2H, Ar-H^2, Ar-H^6), 3.973-3.911 (m, 12H, 2'-OCH_3, 3'-OCH_3, 3-OCH_3, 5-OCH_3), 3.897 (s, 3H, 4-OCH_3), 3.107-2.915 (m, 4H, CH_2CH_2). LC-MS m/z: 411.20 $(M+H)^+$, calcd for $C_{24}H_{26}O_6$: 410.17.

2-((E)-2-(trifluoromethyl)benzylidene)-5-((E)-3,4,5-trimethoxybenzylidene)cyclopentan-1-one (A16): Yellow powder, 67.5% yield, mp 157.3~157.9 °C. ^{1}H-NMR (600 MHz, $CDCl_3$), δ: 7.871 (d, *J*=2.4 Hz, 1H, β-H), 7.772 (d, *J*=7.8 Hz, 1H, Ar-$H^{3'}$), 7.622 (d, *J*=4.2 Hz, 2H, Ar-$H^{5'}$, α-H), 7.578-7.544 (m, 1H, Ar-$H^{6'}$), 7.499-7.432 (m, 1H, Ar-$H^{4'}$), 6.856-6.792 (m, 2H, Ar-H^2, Ar-H^6), 3.931 (s, 9H, 3-OCH_3, 5-OCH_3, 4-OCH_3), 3.105-3.007 (m, 4H, CH_2CH_2). LC-MS m/z: 419.11 $(M+H)^+$, calcd for $C_{23}H_{21}F_3O_4$: 418.14.

2-((E)-3,4-dihydroxybenzylidene)-5-((E)-3,4,5-trimethoxybenzylidene)cyclopentan-1-one (A17): Orange powder, 65.7% yield, mp 184.1~185.5 °C. ^{1}H-NMR (600 MHz, *d*-DMSO), δ: 9.652 (s, 1H, 3'-OH), 9.262 (s, 1H, 4'-OH), 7.374 (s, 1H, β-H), 7.301 (s, 1H, α-H), 7.127 (d, *J*=1.8 Hz, 1H, Ar-$H^{2'}$), 7.034 (dd, *J*=1.2 Hz, *J*=6.6 Hz, 1H, Ar-$H^{6'}$), 7.003 (s, 2H, Ar-H^2, Ar-H^6), 6.855 (d, *J*=7.8 Hz, 1H, Ar-$H^{5'}$), 3.852 (s, 6H, 3-OCH_3, 5-OCH_3), 3.723 (s, 3H, 4-OCH_3), 3.142-3.012 (m, 4H, CH_2CH_2). LC-MS m/z: 383.14 $(M+H)^+$, calcd for $C_{22}H_{22}O_6$: 382.14.

2-((E)-2,5-dimethoxybenzylidene)-5-((E)-3,4,5-trimethoxybenzylidene)cyclopentan-1-one (A18): Yellow powder, 65.6% yield, mp 122.4~123.5 °C. ^{1}H-NMR (600 MHz, $CDCl_3$), δ: 8.002 (s, 1H, β-H), 7.536 (s, 1H, α-H), 7.131 (d, *J*=3.0 Hz, 1H, Ar-$H^{3'}$), 6.938 (dd, *J*=3.0 Hz, *J*=9.0 Hz, 1H, Ar-$H^{6'}$), 6.900 (d, *J*=9.0 Hz, 1H, Ar-$H^{4'}$), 6.865 (s, 2H, Ar-H^2, Ar-H^6), 3.931 (d, *J*=3.6 Hz, 9H, 3-OCH_3, 5-OCH_3, 5'-OCH_3), 3.874 (s, 3H, 2'-OCH_3), 3.836 (s, 3H, 4-OCH_3), 3.114 (s, 4H, CH_2CH_2). LC-MS m/z: 411.20 $(M+H)^+$, calcd for $C_{24}H_{26}O_6$: 410.17.

2-((E)-2-bromobenzylidene)-5-((E)-3,4,5-trimethoxybenzylidene)cyclopentan-1-o

ne (A19): Yellow powder, 72.6% yield, mp 165.2~166.0 °C. ^{1}H-NMR (600 MHz, $CDCl_3$), δ: 7.864 (s, 1H, β-H), 7.691 (d, *J*=7.8 Hz, 1H, Ar-H$^{2'}$), 7.574 (t, *J*=2.4 Hz, 2H, α-H, Ar-H$^{5'}$), 7.384 (d, *J*=7.8 Hz, 1H, Ar-H$^{4'}$), 7.254-7.207 (m, 1H, Ar-H$^{6'}$), 6.863 (s, 2H, Ar-H^2, Ar-H^6), 3.928 (d, *J*=9.0 Hz, 9H, 3-OCH_3, 5-OCH_3, 4-OCH_3), 3.118-3.010 (s, 4H, CH_2CH_2). LC-MS m/z: 429.05 $(M+H)^+$, calcd for $C_{22}H_{21}BrO_4$: 428.06.

2-((E)-4-chlorobenzylidene)-5-((E)-3,4,5-trimethoxybenzylidene)cyclopentan-1-on e (A20): Yellow powder, 80.2% yield, mp 181.2~182.7 °C. ^{1}H-NMR (600 MHz, $CDCl_3$), δ: 7.557-7.539 (m, 4H, Ar-H$^{2'}$, Ar-H$^{6'}$, Ar-H$^{3'}$, Ar-H$^{5'}$), 7.435 (d, *J*=8.4 Hz, 2H, β-H, α-H), 6.869 (s, 2H, Ar-H^2, Ar-H^6), 3.935 (d, *J*=2.4 Hz, 9H, 3-OCH_3, 5-OCH_3, 4-OCH_3), 3.170-3.110 (m, 4H, CH_2CH_2). LC-MS m/z: 385.12 $(M+H)^+$, calcd for $C_{22}H_{21}ClO_4$: 384.11.

2-((E)-3,4-dichlorobenzylidene)-5-((E)-3,4,5-trimethoxybenzylidene)cyclopentan-1-one (A21): Yellow powder, 67.2% yield, mp 153.8~154.3 °C. ^{1}H-NMR (600 MHz, $CDCl_3$), δ: 7.692 (d, *J*=1.2 Hz, 1H, Ar-H$^{6'}$), 7.564-7.518 (m, 2H, β-H, α-H), 7.485 (s, 1H, Ar-H$^{5'}$), 7.430 (dd, *J*=1.8 Hz, *J*=6.6 Hz, 1H, Ar-H$^{2'}$), 6.871 (s, 2H, Ar-H^2, Ar-H^6), 3.938 (d, *J*=1.8 Hz, 9H, 3-OCH_3, 5-OCH_3, 4-OCH_3), 3.184-2.975 (m, 4H, CH_2CH_2). LC-MS m/z: 419.11 $(M+H)^+$, calcd for $C_{22}H_{20}Cl_2O_4$: 418.07.

2-((E)-3,4-difluorobenzylidene)-5-((E)-3,4,5-trimethoxybenzylidene)cyclopentan-1-one (A22): Yellow powder, 63.5% yield, mp 169.0~170.1 °C. ^{1}H-NMR (600 MHz, $CDCl_3$), δ: 7.549 (d, *J*=7.2 Hz, 1H, Ar-H$^{6'}$), 7.501 (s, 1H, β-H), 7.447-7.394 (m 1H, α-H), 7.340 (s, 1H, Ar-H$^{5'}$), 7.245 (t, *J*=18.0 Hz, 1H, Ar-H$^{2'}$), 6.867 (s, 2H, Ar-H^2, Ar-H^6), 3.936 (d, *J*=3.0 Hz, 9H, 3-OCH_3, 5-OCH_3, 4-OCH_3), 3.168-3.106 (m, 4H, CH_2CH_2). LC-MS m/z: 387.16 $(M+H)^+$, calcd for $C_{22}H_{20}F_2O_4$: 386.13.

2-((E)-3,4,5-trimethoxybenzylidene)-5-((E)-3,4,5-trimethoxybenzylidene)cyclopen tan-1-one (A23): Yellow powder, 69.8% yield, mp 203.1~203.4 °C. ^{1}H-NMR (600 MHz, $CDCl_3$), δ: 7.553 (d, *J*=9.0 Hz, 2H, β-H, α-H), 6.871 (s, 4H, Ar-H^2×2, Ar-H^6×2), 3.932 (d, *J*=1.8 Hz, 18H, 3-OCH_3×2, 5-OCH_3×2, 4-OCH_3×2), 3.167 (s, 4H, CH_2CH_2). LC-MS m/z: 441.11 $(M+H)^+$, calcd for $C_{25}H_{28}O_7$: 440.18.

2-((E)-3,4-dimethoxybenzylidene)-5-((E)-3,4,5-trimethoxybenzylidene)cyclopenta n-1-one (A24): Yellow powder, 59.9% yield, mp 168.3~169.5 °C. ^{1}H-NMR (600 MHz, $CDCl_3$), δ: 7.557 (t, *J*=15.9 Hz, 2H, β-H, α-H), 7.265-7.208 (m, 1H, Ar-H$^{6'}$), 7.159 (d, *J*=1.2 Hz, 1H, Ar-H$^{2'}$), 6.969 (d, *J*=8.4 Hz, 1H, Ar-H$^{5'}$), 6.870 (s, 2H, Ar-H^2, Ar-H^6), 3.994-3.884 (m, 15H, 3-OCH_3, 5-OCH_3, 4-OCH_3, 3'-OCH_3, 4'-OCH_3), 3.152 (s, 4H, CH_2CH_2). LC-MS m/z: 411.13 $(M+H)^+$, calcd for $C_{25}H_{26}O_6$: 410.17.

2-((E)-2,3-dichlorobenzylidene)-5-((E)-3,4,5-trimethoxybenzylidene)cyclopentan-1-one (A25): Yellow power, 63.8% yield, mp 181.6~182.1 °C. ^{1}H-NMR (600 MHz, $CDCl_3$), δ: 7.862 (s, 1H, β-H), 7.553 (s, 1H, Ar-H$^{4'}$), 7.479-7.446 (m, 2H, Ar-H$^{5'}$, Ar-H$^{6'}$), 7.250 (s, 1H, α-H), 6.836 (s, 2H, Ar-H^2, Ar-H^6), 3.911 (s, 9H, 3-OCH_3, 5-OCH_3, 4-OCH_3),

3.092 (d, *J*=5.4 Hz, 2H, CH_2), 3.008 (d, *J*=4.8 Hz, 2H, CH_2). LC-MS m/z: 419.17 $(M+H)^+$, calcd for $C_{22}H_{20}Cl_2O_4$: 418.07.

2-((E)-2-fluoro-5-methoxybenzylidene)-5-((E)-3,4,5-trimethoxybenzylidene)cyclopentan-1-one (A26): Yellow powder, 70.3% yield, mp 144.5~145.4 °C. ^{1}H-NMR (600 MHz, $CDCl_3$), δ: 7.774 (s, 1H, β-H), 7.554 (s, 1H, α-H), 7.109-7.093 (m, 1H, Ar-$H^{3'}$), 7.070 (d, *J*=9.0 Hz, 1H, Ar-$H^{4'}$), 6.921-6.895 (m, 1H, Ar-$H^{6'}$), 6.865 (s, 2H, Ar-H^2, Ar-H^6), 3.934 (d, *J*=1.8 Hz, 9H, 3-OCH_3, 5-OCH_3, 5'-OCH_3), 3.848 (s, 3H, 4-OCH_3), 3.152-3.090 (m, 4H, CH_2CH_2). LC-MS m/z: 399.21 $(M+H)^+$, calcd for $C_{23}H_{23}FO_5$: 398.15.

2-((E)-4-(pyrrolidin-1-yl)benzylidene)-5-((E)-3,4,5-trimethoxybenzylidene)cyclopentan-1-one (A27): Orange powder, 61.8% yield, mp 221.4~222.3 °C. ^{1}H-NMR (600 MHz, $CDCl_3$), δ: 7.608 (s, 1H, β-H), 7.547 (d, *J*=7.8 Hz, 2H, Ar-$H^{2'}$, Ar-$H^{6'}$), 7.477 (s, 1H, α-H), 6.865 (s, 2H, Ar-H^2, Ar-H^6), 6.612 (d, *J*=7.8 Hz, 2H, Ar-$H^{4'}$, Ar-$H^{5'}$), 3.927 (d, *J*=6.0 Hz, 9H, 3-OCH_3, 5-OCH_3, 4-OCH_3), 3.380 (s, 4H, CH_2NCH_2), 3.109 (s, 4H, CH_2CH_2), 2.055 (s, 4H, CH_2CH_2). LC-MS m/z: 420.19 $(M+H)^+$, calcd for $C_{26}H_{29}NO_4$: 419.21.

2-((E)-4-hydroxy-3,5-dimethoxybenzylidene)-5-((E)-3,4,5-trimethoxybenzylidene)cyclopentan-1-one (A28): Brown powder, 66.4% yield, mp 194.5~196.0 °C. ^{1}H-NMR (600 MHz, *d*-DMSO), δ: 9.122 (s, 1H, 4'-OH), 7.402 (d, *J*=12.6 Hz, 2H, β-H, α-H), 7.007 (d, *J*=5.4 Hz, 4H, Ar-H^2, Ar-H^6, Ar-$H^{2'}$, Ar-$H^{6'}$), 3.845 (d, *J*=7.2 Hz, 12H, 3-OCH_3, 5-OCH_3, 3'-OCH_3, 5'-OCH_3), 3.724 (s, 3H, 4-OCH_3), 3.145 (s, 4H, CH_2CH_2). LC-MS m/z: 427.18 $(M+H)^+$, calcd for $C_{24}H_{26}O_7$: 426.17.

2-((E)-2,6-dichlorobenzylidene)-5-((E)-3,4,5-trimethoxybenzylidene)cyclopentan-1-one (A29): Yellow powder, 68.5% yield, mp 164.7~164.9 °C. ^{1}H-NMR (600 MHz, $CDCl_3$), δ: 7.544 (s, 1H, β-H), 7.480 (s, 1H, Ar-$H^{4'}$), 7.366 (d, *J*=7.8 Hz, 2H, Ar-$H^{3'}$, Ar-$H^{5'}$), 7.230 (t, *J*=7.8 Hz, 1H, α-H), 6.832 (s, 2H, Ar-H^2, Ar-H^6), 3.905 (d, *J*=3.0 Hz, 9H, 3-OCH_3, 5-OCH_3, 4-OCH_3), 3.059-3.030 (m, 2H, CH_2), 2.715-2.686 (m, 2H, CH_2). LC-MS m/z: 419.05 $(M+H)^+$, calcd for $C_{22}H_{20}Cl_2O_4$: 418.07.

2-((E)-4-bromobenzylidene)-5-((E)-3,4,5-trimethoxybenzylidene)cyclopentan-1-one (A30): Yellow powder, 66.3% yield, mp 189.9~192.8 °C. ^{1}H-NMR (600 MHz, $CDCl_3$), δ: 7.570 (d, *J*=8.4 Hz, 2H, Ar-$H^{3'}$, Ar-$H^{5'}$), 7.523 (d, *J*=9.0 Hz, 2H, Ar-$H^{2'}$, Ar-$H^{6'}$), 7.451 (d, *J*=8.4 Hz, 2H, β-H, α-H), 6.845 (s, 2H, Ar-H^2, Ar-H^6), 3.912 (d, *J*=2.4 Hz, 9H, 3-OCH_3, 5-OCH_3, 4-OCH_3), 3.147-3.049 (m, 4H, CH_2CH_2). LC-MS m/z: 429.14 $(M+H)^+$, calcd for $C_{22}H_{21}BrO_4$: 428.06.

2-((E)-3,5-dichlorobenzylidene)-5-((E)-3,4,5-trimethoxybenzylidene)cyclopentan-1-one (A31): Yellow powder, 65.7% yield, mp 184.3~187.1 °C. ^{1}H-NMR (600 MHz, $CDCl_3$), δ: 7.564 (s, 1H, Ar-$H^{4'}$), 7.459 (s, 2H, β-H, α-H), 7.440 (s, 1H, Ar-$H^{2'}$), 7.384 (s, 1H, Ar-$H^{6'}$), 6.869 (d, *J*=3.6 Hz, 2H, Ar-H^2, Ar-H^6), 3.936 (s, 9H, 3-OCH_3, 5-OCH_3, 4-OCH_3), 3.181-3.120 (m, 4H, CH_2CH_2). LC-MS m/z: 419.06 $(M+H)^+$, calcd for $C_{22}H_{20}Cl_2O_4$: 418.07.

2-((E)-3-methoxybenzylidene)-5-((E)-3,4,5-trimethoxybenzylidene)cyclopentan-1-one (A32): Yellow powder, 69.6% yield, mp 133.8~136.7 °C. ^{1}H-NMR (600 MHz, $CDCl_3$), δ: 7.546 (s, 2H, β-H, α-H), 7.363 (t, *J*=7.8 Hz, 1H, Ar-H$^{5'}$), 7.203 (d, *J*=7.8 Hz, 1H, Ar-H$^{6'}$), 7.126 (s, 1H, Ar-H$^{2'}$), 6.944 (dd, *J*=1.8 Hz, *J*=8.4 Hz, 1H, Ar-H$^{4'}$), 6.848 (s, 2H, Ar-H^2, Ar-H^6), 3.912 (d, *J*=3.6 Hz, 9H, 3-OCH_3, 5-OCH_3, 3'-OCH_3), 3.855 (s, 3H, 4-OCH_3), 3.133 (s, 4H, CH_2CH_2). LC-MS m/z: 381.18 $(M+H)^+$, calcd for $C_{23}H_{24}O_5$: 380.16.

2-((E)-3,5-dimethoxybenzylidene)-5-((E)-3,4,5-trimethoxybenzylidene)cyclopentan-1-one (A33): Yellow powder, 63.6% yield, mp 125.8~128.4 °C. ^{1}H-NMR (600 MHz, $CDCl_3$), δ: 7.544 (d, *J*=5.4 Hz, 2H, β-H, α-H), 6.870 (s, 2H, Ar-H^2, Ar-H^6), 6.773 (d, *J*=1.8 Hz, 2H, Ar-H$^{2'}$, Ar-H$^{6'}$), 6.536 (s, 1H, Ar-H$^{4'}$), 3.933 (d, *J*=3.6 Hz, 9H, 3-OCH_3, 5-OCH_3, 4-OCH_3), 3.858 (s, 6H, 3'-OCH_3, 5'-OCH_3), 3.152 (t, *J*=10.2 Hz, 4H, CH_2CH_2). LC-MS m/z: 411.15 $(M+H)^+$, calcd for $C_{24}H_{26}O_6$: 410.17.

((E)-benzylidene)-5-((E)-2,4,6-trimethoxybenzylidene)cyclopentan-1-one (B9): Orange powder, 78.2% yield, mp 128.5~129.9 °C. ^{1}H-NMR (600 MHz, *d*-DMSO), δ: 7.636 (d, *J*=7.2 Hz, 2H, β-H, α-H), 7.473-7.434 (m, 3H, Ar-H^3, Ar-H^4, Ar-H^5), 7.409-7.387 (m, 2H, Ar-H$^{2'}$, Ar-H$^{6'}$), 6.282 (s, 2H, Ar-H^2, Ar-H^6), 3.821 (s, 3H, 4-OCH_3), 3.802 (s, 6H, 3-OCH_3, 5-OCH_3), 2.971-2.814 (m, 4H, CH_2CH_2). LC-MS m/z: 351.15 $(M+H)^+$, calcd for $C_{22}H_{22}O_4$: 350.15.

2-((E)-2,4,6-trimethoxybenzyl)-5-(3,4,5-trimethoxybenzylidene))cyclopentan-1-one (1): Oil, 68.5% yield. ^{1}H-NMR (500 MHz, $CDCl_3$), δ: 7.538 (s, 1H, Ar-CH=C), 6.431 (s, 2H, Ar-H^2, Ar-H^6), 6.133 (s, 2H, Ar-H$^{3'}$, Ar-H$^{5'}$), 3.855 (s, 3H, 4'-OCH_3), 3.846 (s, 6H, 2'-OCH_3, 6'-OCH_3), 3.827 (s, 4H, CH_2CH_2), 3.819 (s, 6H, 3-OCH_3, 5-OCH_3), 3.804 (s, 3H, 4-OCH_3), 3.768 (s, 3H, CH_2CH). LC-MS m/z: 443.06 $(M+H)^+$, calcd for $C_{25}H_{30}O_7$: 442.20.

2-(2,4,6-trimethoxybenzyl)-5-(3,4,5-trimethoxybenzyl)cyclopentan-1-one (2): Oil, 45.3% yield. ^{1}H-NMR (500 MHz, $CDCl_3$), δ: 6.431 (s, 2H, Ar-H^2, Ar-H^6), 6.133 (s, 2H, Ar-H$^{3'}$, Ar-H$^{5'}$), 3.836-3.855 (m, 9H, 3-OCH_3, 5-OCH_3, 4-OCH_3), 3.827 (s, 3H, 4'-OCH_3), 3.819 (s, 6H, 2'-OCH_3, 6'-OCH_3), 3.799-3.808 (m, 5H, CH_2CHCH_2), 3.761-3.780 (m, 5H, CH_2CHCH_2). LC-MS m/z: 445.06 $(M+H)^+$, calcd for $C_{25}H_{32}O_7$: 444.20.

5.3 Pharmacology

5.3.1 Cell culture

The rat pheochromocytoma cell line (PC12) was purchased from the Cell Storage Center of Wuhan University (Wuhan, China). Primary astrocytes were obtained from the cerebral cortices of Sprague-Dawley (SD) rat pups and cortical neurons from rat fetuses (embryonic day 16–17) were prepared as described by previous authors [48-49]. Cells were

cultured in Dulbecco's Modified Eagle's Medium (DMEM; Gibco, Eggenstein, Germany) containing 10% fetal bovine serum (FBS; Gibco) and antibiotics (1% penicillin–streptomycin; Gibco). The cells were incubated at a temperature of 37°C under a 5% CO_2 atmosphere in a humidified incubator (Thermo Fisher Scientific, Massachusetts, USA).

5.3.2 MTT assay

PC12 cells were seeded in a 96-well plate (NEST Biotechnology Co. LTD., Wuxi, China) at a density of 5×10^3 cells/well and incubated overnight. The cells were exposed to H_2O_2, glucose, glutamate or LPS after treatment with the compounds for 24 h. Then 20 μL 3-[4,5-dimethylthiazol-2-yl]-2,5-diphenyltetrazolium bromide, thiazolyl blue (MTT; 0.5 mg/mL; Sigma, St Louis, Missouri, USA) was added to the culture medium and incubated at 37 °C for 4 h in the dark. Subsequently, the medium was removed carefully and the crystals of formazan were dissolved sufficiently in 120 μL dimethyl sulfoxide (DMSO; Sigma). The optical density (OD) was measured at 490 nm by a microplate reader (Thermo Fisher Scientific, Massachusetts wavelength, USA) and the cell viability was expressed as OD value of the experiment group / OD value of the control group × 100%. The experiment was repeated three times.

5.3.3 Cell colony formation assay

PC12 cells were seeded into 12-well plates (NEST) at a density of 1×10^3 cells/well. After 24 h, cells were treated with the compounds for 24 h, and then exposed to 100 μM H_2O_2. The plates were incubated at 37°C in 5% CO_2 for 6 days. Next, the colony cells were fixed with 4% paraformaldehyde for 40 min and stained with crystal violet for 20 min. The plates were then washed with PBS and dried prior to taking photos.

5.3.4 LDH assay

The amount of LDH released into the medium was determined by using an assay kit according to the manufacturer's protocol from the LDH release cytotoxicity detection kit (Beyotime Institute of Biotechnology, Haimen, China). The changes in absorbance were determined at 490 nm by a microplate reader (Thermo Fisher Scientific). LDH leakage was expressed as the percentage (%) of the total LDH (extracellular + intracellular) activity.

5.3.5 Lipid peroxidation assay

PC12 cells (3×10^5 cells/well) were seeded into 6-well plates (NEST). After cells adhered to the wells overnight, cells were incubated with the compounds for 24 h followed by adding 1 mM H_2O_2 to stimulate cells for 6 h. The malondialdehyde (MDA) level was

measured by an assay kit (Beyotime Institute of Biotechnology, Nanjing, China) according to the manufacturer's instructions. The absorbance was read at a wavelength of 532 nm.

5.3.6 Cell apoptosis assay

PC12 cells (3×10^5 cells/well) were seeded into 6-well plates overnight and then treated with the compounds for 24 h followed by another 6 h H_2O_2 (1 mM) exposure. The rate of cell apoptosis was measured by using an Annexin V-FITC and propidium iodide (PI) double staining kit (BD Biosciences Clontech, San Jose, CA, USA). The procedures were exactly followed according to the manufacturer's instructions and the cell apoptosis was detected by flow cytometry (Becton Dickinson, USA). The results were analyzed by using the Flow Jo analysis program.

5.3.7 ROS assay

Intracellular Reactive Oxygen Species (ROS) generation was measured by dichlorodihydr- ofluorescein diacetate (DCFH-DA; Beyotime Institute of Biotechnology, Shanghai, China). In brief, PC12 cells were seeded into 6-well plates at a density of 3×10^5 per well overnight. Subsequently, cells were pretreated with the compounds for 24 h, followed by another 2 h H_2O_2 (1 mM) exposure. After incubation with 1 μL DCFH-DA (10 μM) for 30 min at 37 °C in the dark, the cells were collected, washed and resuspended in PBS. The intracellular ROS level was quantified by flow cytometry and analyzed with Flow Jo software.

5.3.8 Western blot analysis

PC12 cells were seeded into 6-well culture plates at a density of 3×10^5 cells/ml in 6-well plates and incubated for 48 h at 37 °C. The treated cells were collected and lysed with RIPA lysis buffer (Boster Biological Technology Co. Ltd., Wuhan, China). Then an amount of 80 μg of the protein samples was separated by 10% sodium dodecyl sulfate–polyacrylamide gel (SDS-PAGE) electrophoresis and transferred to a Polyvinylidene Fluoride (PVDF) membrane (Millipore, Massachusetts, USA). The membranes were incubated with the primary antibodies (sc-10789, Santa Cruz Biotechnology, 1:500) and anti-β-actin (AP0060, Bioworld Technology, 1:3000) overnight at 4°C after blocked with 5% non-fat milk at room temperature for 90 min. The next day, the membranes were washed with 1×TBST (Tris-buffered saline, pH 7.6, containing 0.05% Tween 20) three times and incubated with secondary antibody anti-rabbit IgG (1: 1000) for 1 h at room temperature. The blots were imaged by ChemiDoc XRS+system (Bio-Rad,

Hercules, CA), and quantified with Image J software (NIH, Bethesda, MD).

5.3.9 Transfection assay

The short interfering RNA (siRNA) sequences (sense: 5′-GGGUAAGUCGAGAA GUGUUTT-3′, antisense: 5′-AACACUUCUCGACUUACCCTT-3′) targeting Nrf2 was chemically synthesized by Shanghai GenePharma Company. The Nrf2 siRNA or control siRNA was transfected into PC12 cells using Lipofectamine 2000 reagent (Invitrogen, Carlsbad, CA, USA) according to the manufacturer's instructions. The fresh cell culture medium containing FBS was added after 10 h of transfection. Following 48 h knockdown of the Nrf2 expression, the transfected cells were collected and used in further analysis as described in the figure legends.

5.3.10 Experimental animals

Adult male Sprague-Dawley (SD) rats (250-280 g) were obtained from the Beijing Vital River Laboratory Animal Technology Co., Ltd. The rats were fed with a standard laboratory diet and housed under a 12/12 h dark/light cycle in a temperature-controlled room (24 °C). All animal experiments were performed in compliance with the National Institutes of Health guide for the care and use of Laboratory animals (NIH Publications No. 8023, revised 1978) and approved by the Wenzhou Medical University Animal Policy and Welfare Committee.

5.3.11 MCAO model

Focal cerebral ischemia reperfusion model was induced by transient middle cerebral artery occlusion (MCAO) as previously described [50-51]. Briefly, the SD rats were randomly allocated to treatment groups. All surgical procedures were performed after the intraperitoneal injection of 10% chloral hydrate (0.35mL/100 kg; Sinopharm Chemical Reagent Co., Ltd., Shanghai, China) and then an incision was made on the neck to expose the common carotid artery (CCA), the right external carotid artery (ECA) and the internal carotid artery (ICA). A nylon suture was inserted along the cut to the ICA until it occluded the middle cerebral artery (about 18 mm). The suture was pulled out for reperfusion after 2 h of ischemia and the incision was sutured closed. Moreover, the rats were fixated in a stereotaxic apparatus with their head secured firmly in place by ear bars for intracerebroventricular injection. At 2 h before MCAO, the rats received the drugs in a volume of 10 μL using the 25 μL microsyringe and the needle was kept in place for 1 min to prevent backflow after injection. The sham-operated group underwent the same surgical procedure without insertion of the suture.

5.3.12 TTC staining and neurological deficit score

The 2,3,5-triphenyltetrazolium chloride (TTC; Sigma, St. Louis, MO, USA) staining was used to determine the infarct area. The rats were sacrificed by decapitation at 72 h after completion of reperfusion and thereafter the brains were quickly collected and immediately sliced into sections of 2 mm thickness. Subsequently, the brain slices were stained with the 2% TTC at 37 °C for about 30 minutes in the dark and fixed with 4% paraformaldehyde overnight. Infarct sizes were quantified using Image J software (National Institutes of Health, Bethesda, MD, USA). Besides, the neurological score was assessed before animal euthanasia and scoring of each rat was performed within 3 min. Five types of motor neurological findings as follows: 0, no deficits; 1, having difficulty in fully extending the contralateral forelimb; 2, unable to extend the contralateral forelimb; 3, circling to the contralateral side; 4, decreasing level of consciousness; 5, falling to the contralateral side. The higher the neurological score, the more severe the impairment of motor motion.

5.3.13 Statistical analysis

All experiments were repeated more than three times. The results were expressed as means ± standard deviation (SEMs). Statistics were analyzed by using the Student's t-test or one-way analysis of variance for multiple comparisons in GraphPad Pro (GraphPad, San Diego, CA, USA). P values less than 0.05 ($P < 0.05$) were considered as significance.

Supporting Information:

Supplemental Figure S1-S33: LC–MS and 1H NMR spectra of Compound A1-A33.

Supplemental Figure S34: LC–MS and 1H NMR spectra of Compound B9.

Supplemental Figure S35-S36: LC–MS and 1H NMR spectra of Compound 1 and Compound 2.

Author Contributions

Ge Li conducted the biological experiments and prepared the manuscript. Yuantie Zheng and Linya Hu helped the animal experiments. Jiali Yao oversaw and designed the chemistry. Furong Ke and Qunpeng Liu synthesized compounds. Weixiao Feng and Ya Zhao helped to analyze the data. Pencheng Yan, Wenfei He and Hui Deng helped to revise the manuscript. Peihong Qiu helped to identify structures. Jianzhang Wu and Wulan Li designed the study, synthesized compounds and drafted the manuscript.

Acknowledgement

We are grateful to Professor Li Lin of Wenzhou Medical Universtiy for her help. This work was supported by the ZheJiang Province Natural Science Fund of China (Grant Nos. Y19B020043, LY17H160059), and Natural Science Foundation of Wenzhou City (Grant Nos. Y20170158). The Opening Project of Zhejiang Provincial Top Key Discipline of Pharmaceutical Sciences.

References

[1] Buendia I, Michalska P, Navarro E, Gameiro I, Egea J, Leon R. Nrf2-ARE pathway: An emerging target against oxidative stress and neuroinflammation in neurodegenerative diseases. *Pharmacol Ther* **2016**; 157:84-104.

[2] Sivandzade F, Prasad S, Bhalerao A, Cucullo L. NRF2 and NF-κB interplay in cerebrovascular and neurodegenerative disorders: Molecular mechanisms and possible therapeutic approaches. *Redox Biol* **2019**; 21:101059.

[3] Sandberg M, Patil J, D'Angelo B, Weber SG, Mallard C. NRF2-regulation in brain health and disease: implication of cerebral inflammation. *Neuropharmacology* **2014**; 79:298-306.

[4] Ma Q, He X. Molecular basis of electrophilic and oxidative defense: promises and perils of Nrf2. *Pharmacol Rev* **2012**; 64:1055-81.

[5] Seo S, Choi S, Kim K, Kim SM, Park SM. Association between urban green space and the risk of cardiovascular disease: A longitudinal study in seven Korean metropolitan areas. *Environ Int* **2019**; 125:51-7.

[6] Ma H, Campbell BCV, Parsons MW, Churilov L, Levi CR, Hsu TJ, et al. Thrombolysis guided by perfusion imaging up to 9 hours after onset of stroke. *N Engl J Med* **2019**; 380:1795-803.

[7] Staessens S, Denorme F, Francois O, Desender L, Dewaele T, Vanacker P, et al. Structural analysis of ischemic stroke thrombi: histological indications for therapy resistance. *Haematologica* **2019**; 219881.

[8] Liu Y, Min JW, Feng S, Subedi K, Qiao F, Mammenga1 E, et al. Therapeutic role of a cysteine precursor, OTC, in ischemic stroke is mediated by improved proteostasis in mice. *Transl Stroke Res* **2019**; doi: 10.1007/s12975-019-00707-w.

[9] Enomoto M, Endo A, Yatsushige H, Fushimi K, Otomo Y. Clinical effects of early edaravone use in acute ischemic stroke patients treated by endovascular reperfusion therapy. *Stroke* **2019**; 118023815.

[10] Raj L, Ide T, Gurkar AU, Foley M, Schenone M, Li X, et al. Selective killing of cancer cells by a small molecule targeting the stress response to ROS. *Nature* **2011**, 475:231-4.

[11] Bezerra DP, Pessoa C, de Moraes MO, Saker-Neto N, Silveira ER, Costa-Lotufo LV. Overview of the therapeutic potential of piplartine (piperlongumine). *Eur J Pharm Sci* **2013**; 48:453-63.

[12] Sun LD, Wang F, Dai F, Wang YH, Lin D, Zhou B. Development and mechanism investigation of a new piperlongumine derivative as a potent anti-inflammatory agent. *Biochem Pharmacol* **2015**; 95:156-69.

[13] Liu J, Liu W, Lu Y, Tian H, Duan C, Lu L, et al. Piperlongumine restores the balance of autophagy and apoptosis by increasing BCL2 phosphorylation in rotenone-induced Parkinson disease models. *Autophagy* **2018**; 14:845-61.

[14] Wang H, Liu J, Gao G, Wu X, Wang X, Yang H. Protection effect of piperine and

piperlonguminine from Piper longum L. alkaloids against rotenone-induced neuronal injury. *Brain Res* **2016**; 1639:214-27.

[15] Peng S, Zhang B, Meng X, Yao J, Fang J. Synthesis of piperlongumine analogues and discovery of nuclear factor erythroid 2-related factor 2 (Nrf2) activators as potential neuroprotective agents. *J Med Chem* **2015**; 58:5242-55.

[16] Adams DJ, Dai M, Pellegrino G, Wagner BK, Stern AM, Shamji AF, et al. Synthesis, cellular evaluation, and mechanism of action of piperlongumine analogs. *Proc Natl Acad Sci USA* **2012**; 109(38):15115-20.

[17] Zhao C, Cai Y, He X, Li J, Zhang L, Wu J, et al. Synthesis and anti-inflammatory evaluation of novel mono-carbonyl analogues of curcumin in LPS-stimulated RAW 264.7 macrophages. *Eur J Med Chem* **2010**; 45:5773-80.

[18] Wu J, Zhang Y, Cai Y, Wang J, Weng B, Tang Q, et al. Discovery and evaluation of piperid-4-one-containing mono-carbonyl analogs of curcumin as anti-inflammatory agents. *Bioorgan Med Chem* **2013**; 21:3058-65.

[19] Wang Y, Shan X, Dai Y, Jiang L, Chen G, Zhang Y, et al. Curcumin analog L48H37 prevents lipopolysaccharide-Induced TLR4 signaling pathway activation and sepsis via targeting MD2. *J Pharmacol Exp Ther* **2015**; 353:539-50.

[20] Zhang Y, Liu Z, Wu J, Bai B, Chen H, Xiao Z, et al. New MD2 inhibitors derived from curcumin with improved anti-inflammatory activity. *Eur J Med Chem* **2018**; 148:291-305.

[21] Chen L, Li Q, Weng B, Wang J, Zhou Y, Cheng D, et al. Design, synthesis, anti-lung cancer activity, and chemosensitization of tumor-selective MCACs based on ROS-mediated JNK pathway activation and NF-κB pathway inhibition. *Eur J Med Chem* **2018**; 151:508-19.

[22] Sawle P, Moulton BE, Jarzykowska M, Green CJ, Foresti R, Fairlamb IJS, et al. Structure-activity relationships of methoxychalcones as inducers of Heme Oxygenase-1. *Chem Res Toxicol* **2008**, 21, 1484-1494.

[23] Wu J, Ren J, Yao S, Wang J, Huang L, Zhou P, et al. Novel antioxidants' synthesis and their anti-oxidative activity through activating Nrf2 signaling pathway. *Bioorg Med Chem Lett* **2017**; 27:1616-9.

[24] Kareem HS, Ariffin A, Nordin N, Heidelberg T, Abdul-Aziz A, Kong KW, et al. Correlation of antioxidant activities with theoretical studies for new hydrazone compounds bearing a 3,4,5-trimethoxy benzyl moiety. *Eur J Med Chem* **2015**; 103:497-505.

[25] Wu J, Wu S, Shi L, Zhang S, Ren J, Yao S, et al. Design, synthesis, and evaluation of asymmetric EF24 analogues as potential anti-cancer agents for lung cancer. *Eur J Med Chem* **2017**; 125:1321-31.

[26] Qiu P, Zhang S, Zhou Y, Zhu M, Kang Y, Chen D, et al. Synthesis and evaluation of asymmetric curcuminoid analogs as potential anticancer agents that downregulate NF-κB activation and enhance the sensitivity of gastric cancer cell lines to irinotecan chemotherapy. *Eur J Med Chem* **2017**; 139:917-25.

[27] Ying S, Du X, Fu W, Yun D, Chen L, Cai Y, et al. Synthesis, biological evaluation, QSAR and molecular dynamics simulation studies of potential fibroblast growth factor receptor 1 inhibitors for the treatment of gastric cancer. *Eur J Med Chem* **2017**; 127:885-99.

[28] Mohd Aluwi MFF, Rullah K, Yamin BM, Leong SW, Abdul Bahari MN, Lim SJ, et al. Synthesis of unsymmetrical monocarbonyl curcumin analogues with potent inhibition on prostaglandin E2 production in LPS-induced murine and human macrophages cell lines. *Bioorg Med Chem Lett* **2016**; 26(10): 2531-8.

[29] Yao S, Zhou K, Wang J, Cao H, Yu L, Wu J, et al. Synthesis of 2-substituted quinazolines by

CsOH-mediated direct aerobic oxidative cyclocondensation of 2-aminoarylmethanols with nitriles in air. *Green Chem* **2017**; 19:2945-51.

[30] Sun W, Dai L, Yu H, Puspita B, Zhao T, Li F, et al. Monitoring structural modulation of redox-sensitive proteins in cells with MS-CETSA. *Redox Biol* **2019**; 24:101168.

[31] Stamoula E, Vavilis T, Aggelidou E, Kaidoglou A, Cheva A, Mellidis K, et al. Low dose administration of glutamate triggers a non-apoptotic, autophagic response in PC12 cells. *Cell Physiol Biochem* **2017**; 37:1750-8.

[32] Aminzadeh A, Dehpour AR, Safa M, Mirzamohammadi S, Sharifi AM. Investigating the protective effect of lithium against high glucose-induced neurotoxicity in PC12 cells: involvements of ROS, JNK and P38 MAPKs, and apoptotic mitochondria pathway. *Cell Mol Neurobiol* **2014**; 34:1143-50.

[33] Nunez-Villena F, Becerra A, Echeverria C, Briceno N, Porras O, Armisen R, et al. Increased expression of the transient receptor potential melastatin 7 channel is critically involved in lipopolysaccharide-induced reactive oxygen species-mediated neuronal death. *Antioxid Redox Signal* **2011**; 15:2425-38.

[34] Bell KF, Al-Mubarak B, Martel MA, McKay S, Wheelan N, Hasel P, et al. Neuronal development is promoted by weakened intrinsic antioxidant defences due to epigenetic repression of Nrf2. *Nat Commun* **2015**; 6:7066.

[35] Baxter PS, Hardingham GE. Adaptive regulation of the brain's antioxidant defences by neurons and astrocytes. *Free Radical Bio Med* **2016**; 100:147-152.

[36] Wu J, Xi Y, Huang L, Li G, Mao Q, Fang C, et al. A steroid-type antioxidant targeting the Keap1/Nrf2/ARE signaling pathway from the soft coral dendronephthya gigantea. *J Nat Prod* **2018**; 81:2567-75.

[37] Zamponi E, Zamponi N, Coskun P, Quassollo G, Lorenzo A, Cannas SA, et al. Nrf2 stabilization prevents critical oxidative damage in Down syndrome cells. *Aging Cell* **2018**; e12812.

[38] Wu J, Cheng C, Shen L, Wang Z, Wu S, Li W, et al. Synthetic chalcones with potent antioxidant ability on H_2O_2-induced apoptosis in PC12 cells. *Int J Mol Sci* **2014**; 15:18525-39.

[39] Tian S, Ge X, Wu K, Yang H, Liu Y. Ramipril protects the endothelium from high glucose-induced dysfunction through CaMKK /AMPK and Heme Oxygenase-1 activation. J Pharmacol Exp Ther **2014**; 350:5-13.

[40] Gubskiy IL, Namestnikova DD, Cherkashova EA, Chekhonin VP, Baklaushev VP, Gubsky LV, et al. MRI guiding of the middle cerebral artery occlusion in rats aimed to improve stroke modeling. *Transl Stroke Res* **2018**; 9(4):417-25.

[41] Rosell A, Agin V, Rahman M, Morancho A, Ali C, Koistinaho J, et al. Distal occlusion of the middle cerebral artery in mice: are we ready to assess long-term functional outcome? *Transl Stroke Res* **2013**; 4(3):297-307.

[42] Piska K, Gunia-Krzyżak A, Koczurkiewicz P, Wójcik-Pszczoła K, Pękala E. Piperlongumine (piplartine) as a lead compound for anticancer agents-Synthesis and properties of analogues: A mini-review. *Eur J Med Chem* **2018**; 156:13-20.

[43] Oliveira MS, Barbosa MIF, de Souza TB, Moreira DRM, Martins FT, Villarreal W, et al. A novel platinum complex containing a piplartine derivative exhibits enhanced cytotoxicity, causes oxidative stress and triggers apoptotic cell death by ERK/p38 pathway in human acute promyelocytic leukemia HL-60 cells. *Redox Biol* **2019**; 20:182-194.

[44] Sun LD, Wang F, Dai F, Wang YH, Lin D, Zhou B. Development and mechanism investigation of a new piperlongumine derivative as a potent anti-inflammatory agent. *Biochem. Pharmacol* **2015**;

95(3):156-69.

[45] Lu Y, Li C, Chen Q, Liu P, Guo Q, Zhang Y, et al. Microthrombus-targeting micelles for neurovascular remodeling and enhanced microcirculatory perfusion in acute ischemic stroke. *Adv Mater Weinheim* **2019**; e1808361.

[46] Chamorro Á, Dirnagl U, Urra X, Planas AM. Neuroprotection in acute stroke: targeting excitotoxicity, oxidative and nitrosative stress, and inflammation. *Lancet Neurol* **2016**; 15(8):869-81.

[47] Pazos MR, Mohammed N, Lafuente H, Santos M, Martínez-Pinilla E, Moreno E, et al. Mechanisms of cannabidiol neuroprotection in hypoxic-ischemic newborn pigs: role of 5HT(1A) and CB2 receptors. *Neuropharmacology* **2013**; 71:282-91.

[48] Lee EJ, Park JS, Lee YY, Kim DY, Kang JL, Kim HS. Anti-inflammatory and anti-oxidant mechanisms of an MMP-8 inhibitor in lipoteichoic acid-stimulated rat primary astrocytes: involvement of NF-kappaB, Nrf2, and PPAR-gamma signaling pathways. *J Neuroinflamm* **2018**; 15:326.

[49] Malaplate C, Poerio A, Huguet M, Soligot C, Passeri E, Kahn CJF, et al. Neurotrophic effect of fish-lecithin based nanoliposomes on cortical neurons. *Mar Drugs* **2019**; 17(7): 406.

[50] Huang L, Wang J, Chen L, Zhu M, Wu S, Chu S, et al. Design, synthesis, and evaluation of NDGA analogues as potential anti-ischemic stroke agents. *Eur J Med Chem* **2018**; 143:1165-73.

[51] Wang J, Huang L, Cheng C, Li G, Xie J, Shen M, et al. Design, synthesis and biological evaluation of chalcone analogues with novel dual antioxidant mechanisms as potential anti-ischemic stroke agents. *Acta Pharm Sin B* **2019**; 9:335-50.

Graphical abstract: